Impact of changing Arctic sea ice extent, sea ice age, and snow depth on sea salt aerosol from blowing snow and the open ocean for 1980-2017

K. L. Confer[1], L. Jaeglé[1], G. E. Liston[2], S. Sharma[3], V. Nandan[4,5], J. Yackel[4], M. Ewert[6], H. M. Horowitz[7]

[1]Department of Atmospheric Sciences, University of Washington, Seattle, WA, USA

[2]Cooperative Institute for Research in the Atmosphere, Colorado State University, Fort Collins, CO, USA

[3]Environment and Climate Change Canada, Science and Technology Branch, Toronto, Canada

[4]Cryosphere Climate Research Group, Department of Geography, University of Calgary, Calgary, Alberta, Canada

[5]Centre for Earth Observation Science (CEOS), University of Manitoba, Winnipeg, Canada

[6]School of Oceanography, University of Washington, Seattle, WA, USA

[7]Department of Civil and Environmental Engineering, University of Illinois at Urbana-Champaign, Urbana, IL, USA

Corresponding author: Lyatt Jaeglé (jaegle@uw.edu)

Key Points:

- Model predicts pan-Arctic increase in sea salt aerosol emissions by 7-14% decade^{-1} and concentrations by 8-12% decade^{-1} for 1980-2017.
- These trends are due to increasing blowing snow emissions in winter-spring and increasing open ocean emissions in summer-fall.
- Modeled trends are consistent with observed 10-12% decade^{-1} increases in sea salt concentrations at Alert, Canada during winter-spring.

Abstract

We evaluate the effects of rapidly changing Arctic sea ice conditions on sea salt aerosol (SSA) produced by oceanic wave-breaking and the sublimation of wind-lofted salty blowing snow on sea ice. We use the GEOS-Chem chemical transport model to assess the influence of changing extent of the open ocean, multi-year sea ice, first-year sea ice (FYI), and snow depths on SSA emissions for 1980-2017. We combine snow depths from the Lagrangian snow-evolution model (SnowModel-LG) together with an empirically-derived snow salinity function of snow depth to derive spatially and temporally varying snow surface salinity over Arctic FYI. We find that snow surface salinity on Arctic sea ice is increasing at a rate of ~30% decade^{-1} and SSA emissions are increasing at a rate of 7-9% decade^{-1} during the cold season (November – April). As a result, simulated SSA mass concentrations over the Arctic increased by 8-12% decade^{-1} in the cold season for 1980-2017. Blowing snow SSA accounts for more than 60% of this increase. During the warm season (May – October), sea ice loss results in a 12-14% decade^{-1} increase in SSA emissions due to increasing open ocean emissions. Observations of SSA mass concentrations at Alert, Canada display positive trends during the cold season (10-12% decade^{-1}), consistent with our pan-Arctic simulations. During fall, Alert observations show a negative trend (-18% decade^{-1}), due to locally decreasing wind speeds and thus lower open ocean emissions. These significant changes in SSA concentrations could potentially affect past and future bromine explosions and Arctic climate feedbacks.

Plain Language Summary

Suspended sea salt particles affect the climate and chemistry of the atmosphere. The main source of these particles is ocean wave breaking. In polar regions an additional source is the wind lofting of salty snow that is present on top of sea ice. Here we use model simulations to examine how changing Arctic conditions have impacted sea salt particles in the atmosphere. Our simulations show that the concentrations of sea salt particles have increased by more than 8% per decade over the 1980-2017 period. During cold months, this increase is due to saltier blowing snow particles as older sea ice with less salty snow is being replaced by younger sea ice with more salty snow. During warmer months, this increase is the result of larger open ocean emissions as sea ice is melting. These changes in sea salt particles could potentially affect Arctic bromine activation and climate.

1 Introduction

Breaking waves over the open ocean are recognized as the main mechanism for the global production of sea salt aerosol (SSA) (e.g., de Leeuw et al., 2011; Lewis & Schwartz, 2004, and references therein). Additionally, sea ice and snow-sourced SSA have been proposed as significant regional sources of SSA via the sublimation of salty blowing snow on sea ice (Simpson et al., 2007; Yang et al., 2008) and highly saline frost flowers (Domine et al., 2004; Kaleschke et al., 2004; Rankin et al., 2002), as well as wind-driven wave breaking in open leads within the sea ice (May et al., 2016; Nilsson et al., 2001). The role of frost flowers as a direct source of SSA is uncertain; several field and laboratory experiments have demonstrated that frost flowers are difficult to break even under strong wind conditions (Alvarez-Aviles et al., 2008; Roscoe et al., 2011; Yang et al., 2017). Modeling studies including a blowing snow source have been successful in reproducing the cold season (November – April) SSA mass concentrations observed at multiple polar coastal sites, at ice core sites across Greenland, as well as during

Arctic and Antarctic cruises, finding that blowing snow is the dominant source of SSA in polar regions during winter and spring (Huang & Jaeglé, 2017; Rhodes et al., 2017; Yang et al., 2019). Recent field experiments have provided direct evidence of SSA production from blowing snow above sea ice (Frey et al., 2019; Giordano et al., 2018). Snow-sourced SSA likely plays an important role in polar tropospheric ozone and halogen chemistry through the release of active bromine in polar spring which contributes to ozone depletion events (ODEs) (e.g., Choi et al., 2018; Huang et al., 2020; Kalnajs et al., 2013; Marelle et al., 2021; Swanson et al., 2022; Yang et al., 2010).

Over polar regions, the cold season SSA emissions from blowing snow are strongly influenced by meteorological factors (wind speed, temperature, relative humidity) as well as properties of sea ice and snow on sea ice, in particular sea ice extent and snow surface salinity (Frey et al., 2019; Yang et al., 2008). Snow surface salinity is influenced by many factors, including sea ice age and snow depth (Domine et al., 2004). When sea ice retreats during summer and fall, open ocean SSA emissions dominate and are influenced by sea ice extent as well as wind speed and sea surface temperatures (Struthers et al., 2011). Large changes in Arctic climate and sea ice properties have occurred over the last few decades and are expected to continue in the coming decades (Fox-Kemper et al., 2021; Kwok, 2018; Webster et al., 2014). The observed changes include increasing surface temperatures at a rate more than twice the global average, decreasing Arctic sea ice extent at an accelerated rate, thinning sea ice accompanied by a shift to younger ice, and thinning snowpack on sea ice (Meredith et al., 2019 and references therein). There is thus a potential for a significant perturbation of Arctic SSA emissions in response to climate change (Abbatt et al., 2019; Schmale et al., 2021). A quantitative understanding of such changes in SSA is critical since SSA influences radiative forcing and therefore climate both directly by absorbing and scattering sunlight and indirectly by modifying the reflectivity, emissivity, lifetime, and extent of clouds (DeMott et al., 2016; O'Dowd et al., 1997; Struthers et al., 2011).

Is there any evidence for changing SSA mass concentrations over the Arctic sea ice? Long-term observations at high northern latitude sites are scarce and have provided contradicting results so far. Sharma et al. (2019) found that in Alert, Nunavut, Canada sea salt derived Na^+ and Cl^- increased by 19% and 43%, respectively, between 1980 and 2013 during the winter (January-March). These increases were based on the change in the long-term trend factor for the first 5 years relative to the last 5 years and were significant at $p<0.01$. Schmale et al. (2022) examined long-term trends of observed Na^+ concentrations at Alert (1980-2017), Barrow (1998-2014), Zeppelin (1992-2019), and Villum (1991-2017) for the mid-winter season (January-April) and the summer season (June-September) using the seasonal median values. They found no statistically significant trends at any of these sites. Heslin-Rees (2020) reported statistically significant trends in aerosol optical properties observed at Zeppelin Observatory over the past 2 decades, with positive trends in particle light scattering coefficients (+2.6 to +2.9% yr^{-1}) accompanied by negative trends in scattering Ångström exponent (-4.9 to -6.5% yr^{-1}). They interpreted these trends as being caused by increasing transport of SSA from the open ocean to Zeppelin.

A few modeling studies have examined the effect of melting Arctic sea ice on the open ocean source of SSA during summer, with calculated increases in SSA emissions ranging from factors of 1.7 to 10 (Browse et al., 2014; Gilgen et al., 2018; Struthers et al., 2011). For example,

Struthers et al. (2011) found a factor of 4 increase in SSA emissions in a nearly ice-free summer (2100) compared to year 2000. The resulting climate impact ranged from almost no effect (Browse et al., 2014), to a significant negative feedback on climate (Gilgen et al., 2018; Struthers et al., 2011).

To our knowledge, the impact of changing cold season Arctic conditions on SSA emissions from blowing snow has not yet been examined. During the cold season, SSA can act as ice nuclei (DeMott et al., 2016; Wise et al., 2012). Thus, changes in SSA emissions from local sea ice sources could influence the formation, precipitation, and radiative forcing of mixed-phase and ice clouds and thus could influence downward longwave radiative forcing. Any potential changes in sea ice sources of SSA could also affect the occurrence of bromine explosions and ODEs. A recent satellite study by Bougoudis et al. (2020) found that tropospheric BrO columns over Arctic sea ice have been increasing at a rate of +15% decade^{-1} during polar spring. They inferred from comparisons and correlations with sea ice age that the reported changes in the extent and magnitude of tropospheric BrO columns were moderately related to the increase in FYI extent in the Arctic north of 70ºN both temporally and spatially.

One of the key parameters controlling the magnitude of blowing snow-induced SSA emissions is the snow surface salinity. Brines are often present at the snow/sea ice interface and can travel upward through the snow through capillary forces (Geldsetzer et al., 2009; Perovich & Richter-Menge, 1994). This upward migration of brine from the sea ice surface through the snowpack is the dominant source of salinity for snow over newly-formed and first year sea ice (FYI) (Massom et al., 2001; Nandan et al., 2017a; Peterson et al., 2019). Snow over FYI will generally be more saline than over older multi-year ice (MYI) as MYI is desalinated by brine drainage during summer melt cycles (Cox & Weeks, 1974; Krnavek et al., 2012). Other sources of snow salinity include contamination of snow by highly-saline frost flowers, atmospheric deposition of SSA, sea water spraying on the snow cover (especially in marginal ice zones), and sea water flooding caused by heavy snow loading (Abbatt et al., 2012; Domine et al., 2004; Yang et al., 2008). The brine migration height from the sea ice surface through the snowpack has a strong influence on the salinity at the snow surface with thinner snow depths often leading to higher salinities at the surface (Domine et al., 2004; Frey et al., 2019; Massom et al., 2001). As snow depth increases, the salinity of snow decreases, and the influence of atmospheric deposition of SSA can become more important (Krnavek et al., 2012; Nandan et al., 2017b). Over older sea ice types such as second-year ice and MYI, atmospheric deposition of SSA has been proposed as a key main source of snow surface salinity (Huang et al., 2020; Peterson et al., 2019).

Previous modeling of blowing snow SSA emissions assumed spatially and temporally uniform snow surface salinity on FYI and MYI (Frey et al., 2019; Huang et al., 2018, 2020; Huang & Jaeglé, 2017; Rhodes et al., 2017; Yang et al., 2008, 2010, 2019). In this study, we calculate spatially and temporally varying snow surface salinity by combining an empirically-derived snow depth-salinity function with snow depths from a Lagrangian snow-evolution model, SnowModel-LG. We then use the GEOS-Chem chemical transport model to conduct a simulation of SSA over a 38-year period (1980-2017) to quantify the variations in SSA emissions from blowing snow and the open ocean in the Arctic.

The purpose of this study is to understand the impact of decreasing sea ice extent, sea ice age, and snow depths on blowing snow and open ocean emissions of SSA and the resulting changes in SSA mass concentrations throughout the Arctic. The models and observations used in this study are described in Section 2. In Section 3, we examine the response of snow surface salinity to changing Arctic conditions. The resulting evolution of SSA emissions and mass concentrations are discussed in Section 4. We compare modeled trends in SSA mass concentrations to observations at Alert, Canada in Section 5. Conclusions are presented in Section 6.

2 Models and Observations

2.1 GEOS-Chem chemical transport model

We use the GEOS-Chem (v13.0.2) global chemical transport model (Bey et al., 2001) driven by the Modern-Era Retrospective analysis for Research and Applications, version 2 (MERRA-2) assimilated meteorological fields (Gelaro et al., 2017), which have a native horizontal resolution of 0.5º latitude by 0.625º longitude with 72 vertical levels. SSA emissions are calculated at this native horizontal resolution using the Harmonized Emission Component (HEMCO) (Keller et al., 2014). For faster computation, we regridded the HEMCO SSA emissions and MERRA-2 meteorological fields to a 2º × 2.5º horizontal resolution and 47 vertical levels with merged levels above 80 hPa to conduct the SSA simulations within GEOS-Chem.

As wind-driven ocean waves break, they entrain air bubbles which rise to the ocean surface where they burst and generate SSA. The open-ocean emissions of SSA in GEOS-Chem are a function of wind speed and sea surface temperature (SST) as described in Jaeglé et al. (2011). We assume that SSA are emitted from open leads within the sea ice with the same efficiency as over the open ocean. Huang and Jaeglé (2017) implemented blowing snow SSA emissions in GEOS-Chem based on the parameterization of Yang et al. (2008, 2010). The SSA production from blowing snow is a function of relative humidity, temperature, age of snow, snow salinity, and wind speed. The Yang et al. (2008, 2010) parameterization was originally based on blowing-snow measurements above ice sheets (Budd, 2013; Mann et al., 2000; Nishimura & Nemoto, 2005) and the Canadian Prairies (Déry & Yau, 1999, and references therein) but have since been evaluated against direct observations of SSA production from blowing snow above sea ice (Frey et al., 2019). The minimum wind speed needed to saltate and suspend snow particles from the sea ice surface is temperature dependent. The size distribution of suspended blowing snow particles follows a two-parameter gamma distribution (Yang et al., 2008, and references therein). As in Huang and Jaeglé (2017), we assume a mean snow age of 3 days for the Arctic.

In our previous work (Huang et al., 2018, Huang et al., 2020), we assumed a uniform salinity of 0.1 practical salinity units (psu) for snow on FYI and 0.01-0.05 psu for snow on MYI in the Arctic. The MERRA-2 boundary conditions for sea ice concentrations are described in Gelaro et al. (2017) and are derived from the monthly 1º product from Taylor et al. (2000) prior to 1982, the daily 1/4º product from Reynolds et al. (2007) for 1982 until March 2006, and the daily 1/20º product from Donlon et al. (2012) after March 2006. In our previous work, we inferred the location of MYI sea ice based on the preceding summertime minimum sea ice extent from MERRA-2. The location of MYI was then assumed to be invariant until the next summer. We have updated this approach to instead use the EASE-Grid Sea Ice Age, Version 4 product

distributed at the National Snow & Ice Data Center (NSIDC, Tschudi et al., 2019). This dataset provides weekly Arctic sea ice age since January 1984 and is described in Tschudi et al. (2020). For years prior to 1984, we assign MYI extent based on the minimum sea ice extent from MERRA-2 at the end of summer of the previous year.

Dry deposition of SSA over land follows the size-segregated scheme described in Zhang et al. (2001). The dry deposition velocity over the ocean is calculated based on the Slinn and Slinn (1980) deposition model for natural waters. Over snow and ice surfaces, Fisher et al., 2011 implemented a dry deposition velocity of 0.03 cm s^{-1} based on the measurements of Nilsson et al. (2001). The wet deposition scheme includes convective updraft scavenging, rainout, and washout from precipitation (Liu et al., 2001), and snow scavenging (Wang et al., 2011). For this work, we track SSA mass in two size bins, submicron (r_{dry} = 0.01–0.5 μm) and supermicron (r_{dry} = 0.5–8 μm), except in the comparison to in situ mass concentrations of SSA for which we use r_{dry} = 0.01–0.3 μm and r_{dry} = 0.3–3 μm as described in Huang and Jaeglé (2017).

2.2 SnowModel-LG

SnowModel-LG is a prognostic Lagrangian ice-parcel tracking snow model that accounts for physical snow processes including rainfall, snowfall, sublimation from static surfaces and blowing snow, blowing snow redistribution, snow density evolution, and snowpack metamorphosis (Liston et al., 2020). In this application, the model was forced by precipitation, 2 m air temperature, wind speed and direction from two reanalysis products (MERRA-2 and ERA5) and by weekly ice motion vectors (Tschudi et al., 2019; Tschudi et al., 2020).

Within its Lagrangian framework, SnowModel-LG followed over 61,000 ice parcels in the Arctic and was used to produce daily, pan-Arctic, snow depth distribution on a 25x25 km grid from August 1980 through July 2018 (Liston et al., 2020). Stroeve et al. (2020) evaluated the SnowModel-LG simulation against several data sets including Operation IceBridge, ice mass balance buoys, MagnaProbes, and passive microwave estimates. They found the model captured observed spatial and seasonal variability in snow depth accumulation, while also showing statistically significant declines in snow depth since 1980 during the cold season. For application in our study, we use SnowModel-LG forced by MERRA-2 and regridded the SnowModel-LG daily snow depth to the native MERRA-2 resolution.

2.3 Implementation of snow depth-dependent snow surface salinity

We use in situ observations of snow salinity on Arctic sea ice reported in four different studies (Ewert et al., 2013; Krnavek et al., 2012; Nandan et al., 2017b; Peterson et al., 2019). More than half of the samples used in our work were collected during nine field campaigns in the Canadian Arctic (see Figure 1a) as summarized in Nandan et al. (2017b). These samples were taken in April-May between 2004 and 2017, on both undeformed and slightly deformed FYI. Ewert et al. (2013) collected snow salinity samples from landfast FYI near Utqiaġvik/Barrow, AK, during February 2010 and March 2011. Krnavek et al. (2012) collected snow surface samples during March and April in 2004, 2005, and 2007 on thin and thick FYI, as well as over MYI. Lastly, Peterson et al. (2019) collected snow samples over both FYI and MYI in regions across the Arctic Ocean accessed via aircraft in April-May 2013, February 2014, and April 2014.

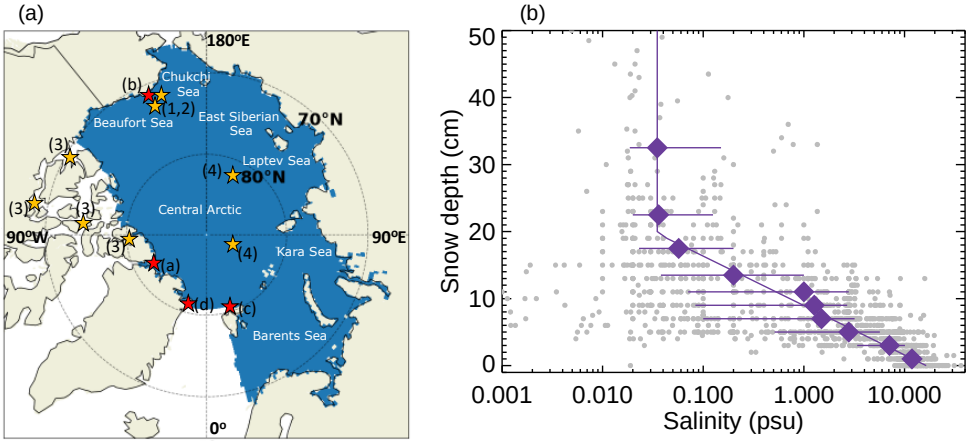

Figure 1. (a) Locations of snow salinity observations (orange stars: (1) Ewert et al., 2013; (2) Krnavek et al., 2012; (3) Nandan et al., 2017b; (4) Peterson et al., 2019) and of the surface stations with SSA mass concentrations observations (red stars: (a) Alert, (b) Barrow/Utqiaġvik, (c) Zeppelin, (d) Villum) used in this study. The blue region constitutes the Arctic region considered in this study. This region includes the Central Arctic as well as the Beaufort, Chukchi, East Siberian, Laptev, Kara, and Barents Seas. (b) In situ observations of snow salinity (filled grey circles) as a function of snow depth. These observations were collected on FYI. 0 cm on the y-axis represents the snow/sea ice interface. The purple diamonds correspond to the medians of the observations separated into 2-5 cm snow thickness bins. Purple horizontal bars correspond to the 25th and 75th percentiles of each bin. The purple line is the fit to the binned median values (Equation 1).

Figure 1b shows all 1440 individual in situ snow salinity observations displayed as a function of snow depth. We only show observations collected over FYI. Very high salinity values occur within the first 4 cm above the sea ice surface, often exceeding 5 psu and reaching up to 35 psu, and then salinity rapidly decreases with increasing snow depth until 20 cm above the snow/ice interface. Above 20 cm salinities tend to be much lower, typically <0.05 psu, but sometimes reaching higher values. This overall behavior is consistent with upward migration of brine from the sea ice surface up to 20 cm (Domine et al., 2004; Geldsetzer et al., 2009; Nandan et al., 2017a).

We separate the salinity observations in ten snow depth bins and calculate the median salinity for each bin: 0-2 cm (11.9 psu, n=239 observations), 2-4 cm (7.1 psu, n=220), 4-6 cm (2.8 psu, n=222), 6-8 cm (1.5 psu, n=148), 8-10 cm (1.27 psu, n=104),10-12 cm (1 psu, n=88), 12-15 cm (0.2 psu, n=129), 15-20 cm (0.057 psu, n=65), 20-25 cm (0.036 psu, n=51), 25 cm and above (0.035 psu, n=35). The top two bins representing observations >20 cm have similar medians ~0.035 psu and we use this value as our minimum salinity of surface snow over FYI. For the bins below 20 cm, we fit the median salinities with an exponential function of snow depth: salinity=16.47 exp(-0.312 z), where z is snow depth in cm. We use medians instead of means because the distribution of snow salinities is skewed towards high values.

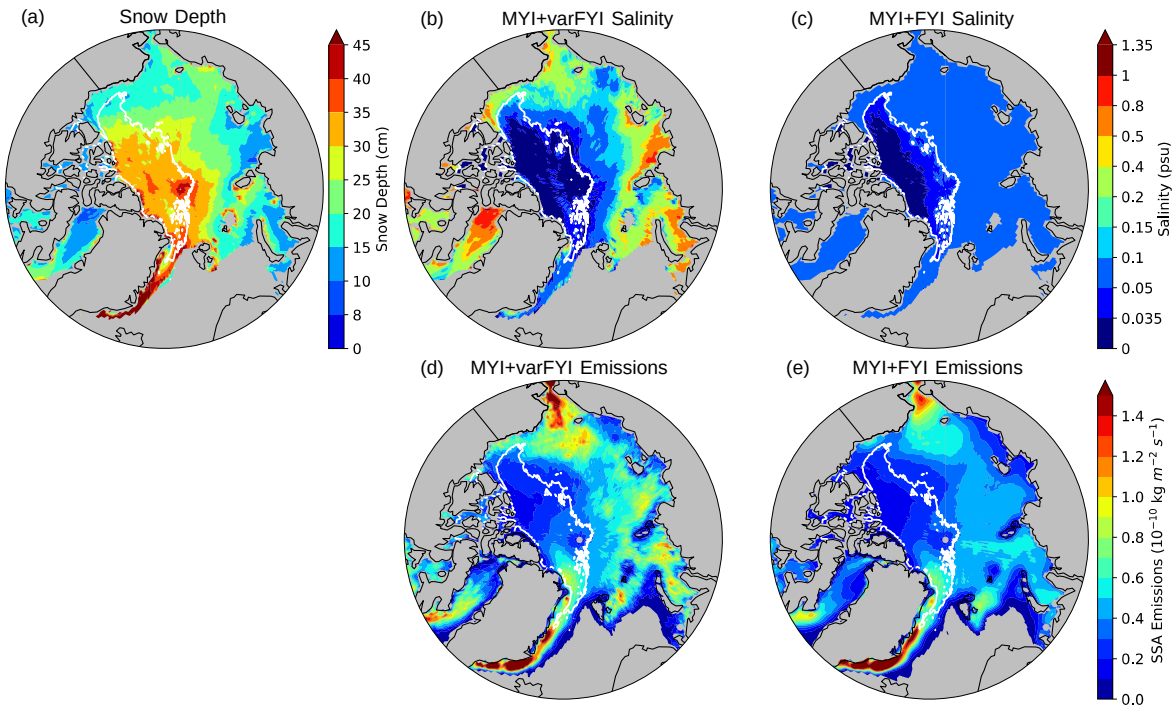

Figure 2. Spatial distribution of (a) SnowModel-LG snow depth over sea ice, (b) snow surface salinity calculated with Equation 1, (c) fixed snow salinity assuming 0.1 psu on FYI and 0.035 psu on MYI, (d) blowing snow SSA emissions from the variable salinity simulation (MYI+varFYI), and (e) blowing snow SSA emissions from the fixed salinity simulation (MYI+FYI) for February-April 2005-2014. The mean snow salinity excludes areas where snow depths are below the snow holding depth of 8 cm (see discussion in Section 2.3). The white contour represents mean MYI extent.

We combine this empirical exponential function with daily snow depths from SnowModel-LG (Section 2.2) to calculate snow surface salinity. This expression leads to very high salinities for thin snow cover, which generally occurs over newly formed sea ice in the fall. Observations show that the surface of young sea ice is covered by a thin, highly saline liquidlike skim, thus the snow itself is highly saline but also contains large amounts of liquid brine (Drinkwater & Crocker, 1988). This slushy brine-wetted snow is unlikely to be lifted by winds. To account for this, we implement a snow-holding depth, which is the snow depth that must be exceeded before snow becomes available for wind transport (Liston & Sturm, 2002). We conducted sensitivity studies varying the snow-holding depth between 2 and 10 cm and evaluated our results against observations of SSA mass concentrations (section 2.5). Based on these sensitivity studies, we found that a snow-holding depth of 8 cm is most consistent with observations. We thus use this 8 cm snow-holding depth to calculate blowing snow SSA emissions. We apply the following equation to derive spatially and temporally varying snow salinity over sea ice:

$$\begin{cases} salinity_{FYI} = 16.47exp(-0.312\ z)\ psu, 8 < z < 20cm \\ salinity_{FYI} = 0.035\ \text{psu}, \quad z \geq 20\ \text{cm} \\ salinity_{MYI} = 0.035\ psu \end{cases} \qquad \text{Equation 1}$$

where z is snow depth in cm. Observations of snow surface salinity over MYI are scarcer than for FYI. Krnavek et al. (2012) reported mean values of 0.01 psu, while Peterson et al. (2019) reported values ranging from 0.02 psu for snowpack deeper than 17 cm to 0.15 psu for shallower snowpack. Combining the observations from these two studies (61 samples), we find no clear dependence on snow depth. For simplicity, we assume a salinity of 0.035 psu on MYI, the same value as for deeper snowpack on FYI (Equation 1). Figure 2b shows the spatial distribution of snow surface salinities calculated by applying Equation 1 to snow depths from SnowModel-LG (Figure 2a) for February-April 2005-2014. The salinities displayed in this figure exclude areas where snow depths are below the snow holding depth of 8 cm, and thus reflect salinities that are relevant for blowing snow SSA emissions. The largest salinities (>0.5 psu) occur over FYI in regions with snow depths less than 15 cm located mainly in the Kara, Chukchi, and Laptev Seas. The resulting mean snow surface salinity over FYI is 0.18 psu. Figure 2c shows the mean salinity obtained for the same period if we assume a fixed salinity of 0.1 psu over FYI and a salinity of 0.035 psu over MYI.

2.4 Simulations conducted as part of this work

We conduct four GEOS-Chem SSA simulations for 1980-2017 : (1) a baseline simulation in which the only source of SSA is from the open ocean and areas of open water within the sea ice (together referred to as "OO"); (2) a simulation that includes open ocean and blowing snow SSA sources on MYI (referred to as "OO+MYI"), where only MYI is a source of blowing snow, assuming a fixed salinity of 0.035 psu; (3) a simulation that includes open ocean and blowing snow SSA sources on both FYI and MYI (referred to as "OO+MYI+FYI"), for which we assume fixed snow surface salinity of 0.1 psu on FYI and 0.035 psu on MYI; (4) a simulation with open ocean and blowing snow SSA sources assuming spatially and temporally variable salinity on FYI (Section 2.3) and fixed salinity (0.035 psu) on MYI ("OO+MYI+varFYI"). Together, these simulations allow us to separate the individual impact of SSA emissions from the open ocean, MYI (by difference between "OO+MYI" and "OO"), FYI with fixed salinity (difference between "OO+MYI+FYI" and "OO+MYI"), and FYI with variable salinity (difference between "OO+MYI+varFYI" and "OO+MYI").

The simulations use the same assumptions for the blowing snow parameterization as in our previous work (Section 2.1), apart from snow surface salinity and the number of particles produced per snowflake (N). The value of N influences the size distribution SSA produced from blowing snow but does not change the total emissions. For the OO+MYI+FYI and OO+MYI simulations, we use N=5 as in Huang & Jaeglé (2017). This choice was based on comparisons to wintertime observations of submicron and supermicron SSA at Utqiaġvik/Barrow. The OO+MYI+varFYI simulation results in higher mean salinities and thus a shift of blowing snow SSA to larger sizes. In order to reproduce the wintertime observations of submicron and supermicron SSA at Barrow, we increase N to a value of 10 for that simulation.

Table 1 summarizes the annual mean budgets for individual SSA sources as calculated in GEOS-Chem for 2005-2014 for the Arctic region defined in Figure 1a. The total (0.01–8 μm) blowing snow source is 0.3 Tg/yr for MYI, 1.5 Tg/yr for MYI+FYI and 2.5 Tg/yr for MYI+varFYI. Blowing snow emissions from the MYI+varFYI simulation (Figure 2d) are enhanced in regions with higher salinity values (Figure 2b). The salinity also affects the size distribution of the blowing snow SSA emissions, with larger SSA at higher salinities (see equation 7 in Yang et al.,

2018). Indeed, the ratio between submicron and supermicron SSA emissions decreases from 1.0 for the MYI simulation, to 0.75 for the MYI+FYI simulation, and 0.47 for the MYI+varFYI simulation (Table 1). The open ocean accounts for most of the emissions and surface mass concentrations of supermicron SSA over the Arctic (OO: 13.5 Tg/yr and 1.4 μg/m^3; MYI+FYI: 0.9 Tg/yr and 0.2 μg/m^3; MYI+varFYI: 1.7 Tg/yr and 0.4 μg/m^3), however submicron SSA are dominated by blowing snow (OO: 0.2 Tg/yr and 0.2 μg/m^3; MYI+FYI: 0.6 Tg/yr and 0.6 μg/m^3; MYI+varFYI: 0.8 Tg/yr and 0.8 μg/m^3).

Table 1. Annual mean Arctic (region defined in Figure 1a) SSA budgets for submicron (0.01-0.5 μm) and supermicron (0.5-8 μm) SSA originating from the open ocean (OO), blowing snow over MYI (MYI), blowing snow over both MYI and FYI with fixed salinity (MYI+FYI), and blowing over MYI and FYI with variable salinity (MYI+varFYI) for 2005-2014.

	Open Ocean: OO			MYI			MYI+FYI			MYI+varFYI		
	0.01 - 0.5 μm	0.5 - 8 μm	Total	0.01 - 0.5 μm	0.5 - 8 μm	Total	0.01 - 0.5 μm	0.5 - 8 μm	Total	0.01 - 0.5 μm	0.5 - 8 μm	Total
Emission Tg yr^{-1}	0.2	13.5	13.8	0.2	0.2	0.3	0.6	0.9	1.5	0.8	1.7	2.5
Dry Deposition Tg yr^{-1}	0.0	4.3	4.3	0.04	0.1	0.1	0.1	0.3	0.4	0.1	0.6	0.8
Wet Deposition Tg yr^{-1}	0.2	7.7	7.9	0.03	0.1	0.1	0.1	0.4	0.5	0.1	0.8	0.9
Lifetime days	3.0	0.3	0.4	6.5	0.5	2.6	6.6	0.5	2.0	7.0	0.5	1.6
Burden Gg	1.7	10.5	12.2	1.2	0.2	1.4	4.3	0.9	5.2	5.4	1.8	7.3
Surface Concentration μg m^{-3}	0.2	1.4	1.5	0.2	0.0	0.2	0.6	0.2	0.8	0.8	0.4	1.1

2.5 Model evaluation with *in situ* observations of SSA mass concentrations at Arctic sites

Figure 3 compares our model simulations to *in situ* observations of SSA mass concentrations at four Arctic sites: Alert, Nunavut, Canada (Sharma et al., 2019); Villum Research Station, Greenland (Tøseth et al., 2012); Barrow/Utqiaġvik, Alaska, USA (Quinn et al., 2002) and Zeppelin Observatory, Svalbard, Norway (Tørseth et al., 2012). The location of these sites is indicated in Figure 1a (red stars). To conduct our evaluation, we use observations for 2005–2014, except for Villum, which only has observations starting in 2008. At Barrow/Utqiaġvik Na^+ mass concentrations are available for both submicron and supermicron aerosol, while all the other sites measure total mass concentrations. The aerosol sampling frequency ranges from daily (Zeppelin, submicron at Barrow/Utqiaġvik), to weekly (Alert, Villum). The Barrow/Utqiaġvik supermicron Na^+ observations have variable sampling times (1-4 weeks). In the winter months, the coastlines near these sites are mostly covered by sea ice. For comparison between the GEOS-Chem model and the observations, we convert observed Na^+ mass concentrations to SSA mass concentrations using a factor of 3.256 based on the mass ratio of Na^+ in seawater (Riley and Chester, 1971). This factor is similar to the ratios of 3.24-3.278 reported by Krnavek et al. (2012) for snow on FYI.

Observations at all four sites display a similar seasonal cycle, with enhanced SSA mass concentrations (1-1.5 μg m^{-3}) during the cold season (November – April), and lower concentrations (< 0.5 μg m^{-3}) during the warm season (May – October) (Figure 3). The OO simulation underestimates the wintertime maximum at Barrow/Utqiaġvik, Alert and Villum by factors of 3-10 but reproduces concentrations during the warm season. At Zeppelin, the OO simulations overestimates the observations during the cold season. When a blowing snow source is added to GEOS-Chem (OO+MYI+FYI and OO+MYI+varFYI), the model can successfully reproduce the seasonal cycle and agreement with observations is improved at Barrow/Utqiaġvik, Alert and Villum. However, at Zeppelin the blowing snow source leads to a larger overestimate of the observations. The higher elevation of Zeppelin (475 m above sea level) results in more

influence from the free troposphere and aerosol-cloud interactions (Freud et al., 2017), which together with the complex nearby topography might not be captured by the model. Overall, both blowing snow simulations capture the observed SSA seasonal cycle reasonably well. The addition of temporally and spatially varying salinity on FYI increases the modeled concentrations during the cold season by 0.1-0.3 μg m^{-3}. None of these stations are located close to the high salinity areas Figure 2b) predicted by our empirical salinity-snow depth model in the Eastern Arctic, and thus the modeled influence of variable salinity is relatively small at these four locations. Overall, our finding of a strong source of SSA from blowing snow during cold months at these sites is consistent with the backtrajectory analysis of Moschos et al. (2022) showing that SSA at these sites originates from the sea ice covered Beaufort, Kara, Laptev, and Chukchi Seas as well as the Arctic Ocean.

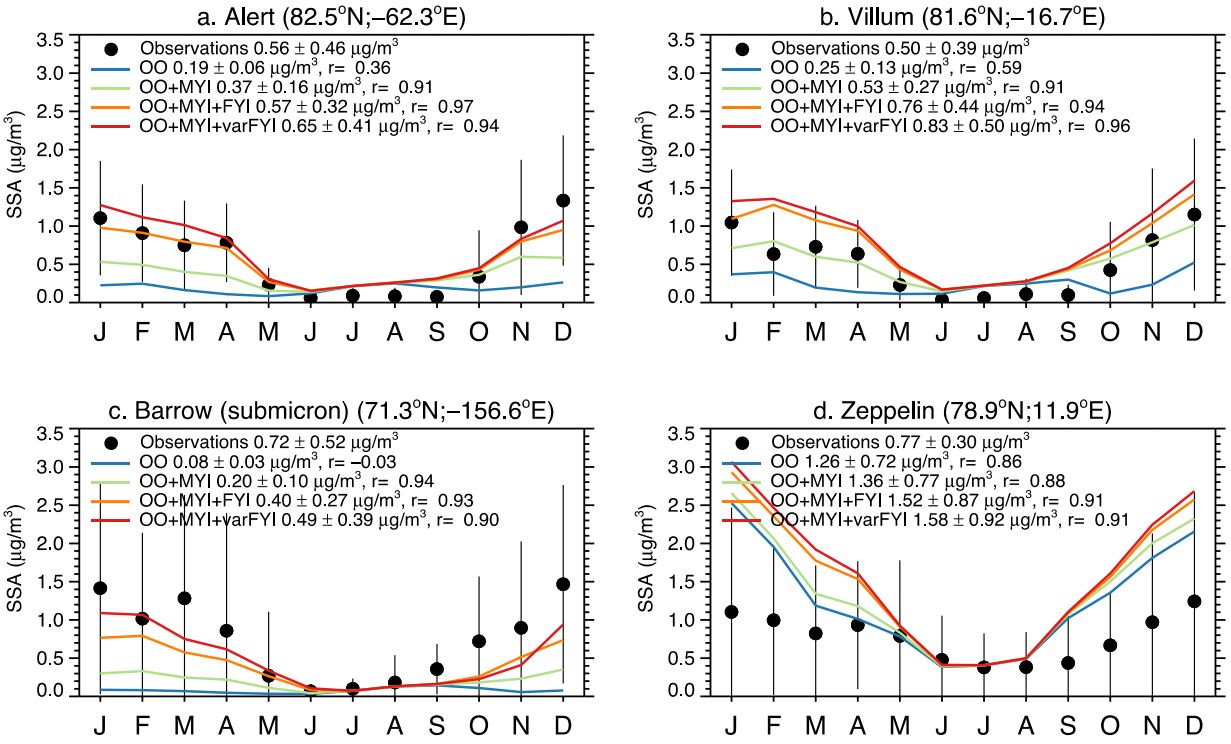

Figure 3. Monthly mean mass concentrations of SSA at: a) Alert, b) Villum, c) Barrow/Utqiaġvik, d) Zeppelin. All observations and model results are for 2005–2014 (except for Villum, where observations are available starting in 2008). The observed SSA concentrations are indicated with filled black circles. The black vertical lines correspond to the standard deviations of monthly means observations. The four GEOS-Chem simulations are shown with solid lines (OO: blue; OO+MYI: green, OO+MYI+FYI: orange; OO+MYI+varFYI: red). For each individual panel, the legend lists mean concentrations and standard deviations, as well as the correlation coefficient between model and observations.

2.6 Trend and significance calculations

We calculate trends in snow depth, snow surface salinity, SSA emissions, and SSA mass concentrations using the Theil-Sen slope from the non-parametric Mann-Kendall test. The test has been widely used with environmental data including Arctic data sets (Collaud Coen, 2020ab; Heslin-Rees et al., 2020; Lam et al., 2022; Skov et al., 2020; Tunved & Ström, 2019). We define

a trend to be significant if the *p*-value is less than or equal to 0.05. We express the trends in % decade^{-1}, relative to the 1980-2017 mean.

These trends are calculated for the means of each season, which we define in this paper based on the seasonality of observed SSA mass concentrations in the Arctic (Figure 3): winter (November, December, January: NDJ), spring (February, March, April: FMA), summer (May, June, July: MJJ) and fall (August, September, October: ASO). We acknowledge that there are different definitions of seasons in the Arctic, which can vary depending on the perspective chosen (e.g., polar day/night, temperature, sea ice evolution, haze transport). For example, Sharma et al. (2019) define winter as JFM and spring as AM. Given our focus on SSA and its sources in the Arctic, here we choose to group months based on the seasonal cycle of SSA observations.

3 Response of snow surface salinity to changing Arctic sea ice conditions for 1980-2017

Figure 4a shows the 1980-2017 timeseries of MERRA-2 monthly mean sea ice area in the Arctic (region defined in Figure 1a). It highlights the accelerated decline of the annual sea ice minimum and the major melting events that took place in 2007 and 2012 (Parkinson & Comiso, 2013). Most notably, the figure shows the rapid decline of MYI. During cold months, when blowing snow emissions constitute a significant source of SSA, sea ice area has declined slightly but more importantly, FYI has increased, replacing older MYI. Figure 4b shows the snow depths over FYI predicted by SnowModel-LG. These thinning snow depths are due to the delayed onset of sea ice formation in fall reducing snow accumulation as snow falls in the ocean instead of on sea ice (Mallett et al., 2021; Markus et al., 2009; Stroeve et al., 2020; Stroeve & Notz, 2018; Webster et al., 2014). We find that snow salinity is increasing in both the MYI+FYI and MYI+varFYI blowing snow simulations (Figure 4c). The increase in salinity in the MYI+FYI simulation is due to the replacement of older, less saline MYI with FYI. The increase is much stronger in the MYI+varFYI simulation because of the added effect of thinning snowpack on FYI. In the MYI+varFYI simulation, salinity is highest in late fall when FYI begins to freeze, and the snowpack is thin. Salinity then decreases throughout the cold season as the snowpack becomes thicker.

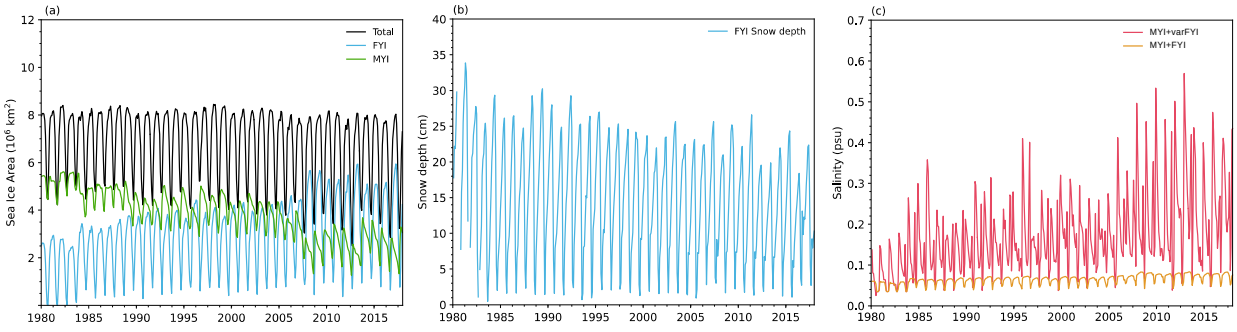

Figure 4. Monthly mean Arctic (a) sea ice area in units of 10^6 km^2, (b) snow depth over FYI in units of cm, and (c) snow surface salinity in units of psu for 1980-2017. The Arctic region is defined in Figure 1a. Panel (a) includes total sea ice area (black), FYI area (light blue), and MYI area (green). Panel (c) shows snow surface salinity for the fixed salinity (MYI+FYI) simulation (orange) and variable salinity (MYI+varFYI) simulation (red). Note that the MYI+varFYI salinity only includes regions with snow depth above the snow-holding depth of 8 cm (Section 2.3).

Figure 5 shows the spatial and temporal evolution of seasonally averaged snow depths for 1980-2017. We focus on winter (NDJ) and spring (FMA) months, which are the most relevant for blowing snow SSA emissions. At the beginning of the time period (1980-1984, Figure 5ab) most of the Arctic sea ice is dominated by snow depths greater than 15-20 cm in winter (>25 cm in spring). At the end of the period (2013-2017) these deeper snow depths are limited to the central Arctic, with thinner snow depths (<15 cm) occurring in the East Siberian, Laptev, Chukchi, and Beaufort Seas, mostly constrained to FYI. We find that mean Arctic snow depths over sea ice have decreased at a rate of -0.79 cm decade^{-1} (-4% decade^{-1}) in winter (Figure 5d) and -0.98 cm decade^{-1} (-3.5% decade^{-1}) in spring (Figure 5h). The largest negative trends (-4 to -6 cm decade^{-1}) occur in areas where FYI has replaced MYI (Figure 5c,g), in the Beaufort, Chukchi, East Siberian, and Laptev Seas. In some regions, such as the Central Arctic, snow depth trends are positive but are not statistically significant. These trends in snow depths from SnowModel-LG are discussed in more detail in Stroeve et al. (2020) and are consistent with Webster et al. (2014).

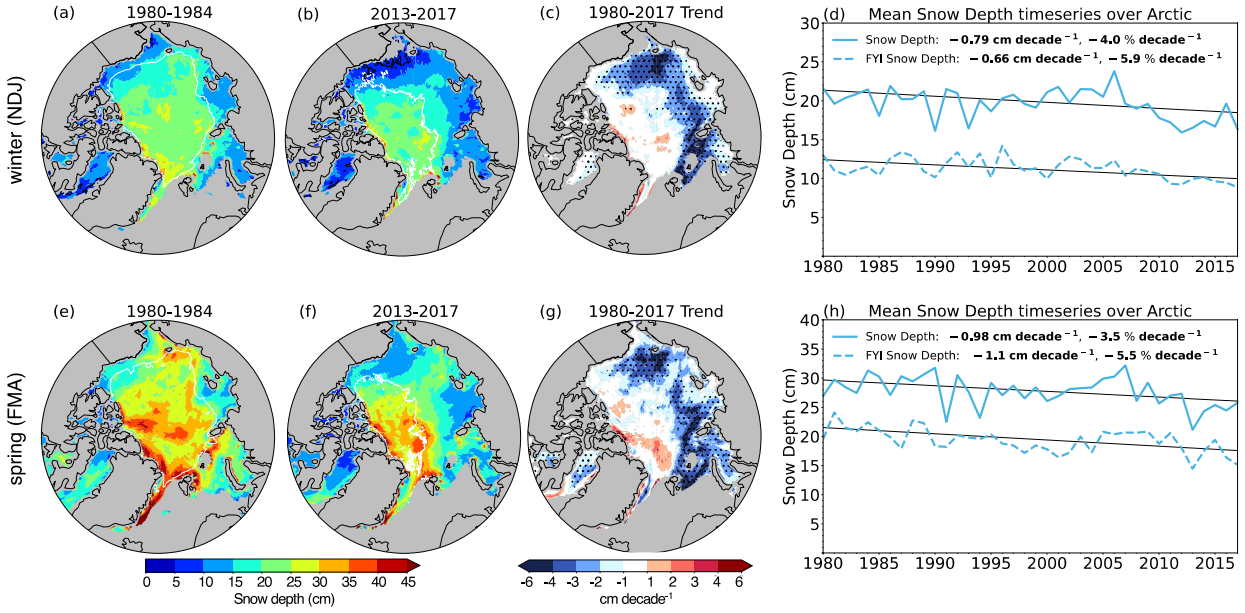

Figure 5. Seasonally averaged SnowModel-LG snow depths for winter (NDJ; top row) and spring (FMA; bottom row). Average snow depth for (a, e) 1980-1984 and (b, f) 2013-2017. (c, g) Spatial distribution of trends (cm decade^{-1}) for 1980-2017. Black dots indicate statistically significant trends. The white contours on (a, b, e, f) show the mean extent of MYI. (d, h) Timeseries of Arctic snow depth over all sea ice (solid blue line) and FYI only (dashed blue line). The legend lists the trend in cm decade^{-1} and % decade^{-1}. Statistically significant trends are indicated in bold in the legend.

Figure 6 shows the spatial and temporal evolution of snow salinity. Over the 1980-2017 period, we find that winter snow surface salinity in the MYI+varFYI simulation increases by 36% decade^{-1} (0.027 psu decade^{-1}) while the salinity in the MYI+FYI simulation increases by 11% decade^{-1} (0.0047 psu decade^{-1}, Figure 6d), with similar trends in spring. These trends are statistically significant. The largest increases in snow surface salinity occur in regions where FYI has replaced MYI and where snow depths are thinning, such as the East Siberian, Laptev, Kara, and Barents Seas (Figure 6c, g). By comparison between the salinity predicted in the MYI+FYI

and MYI+varFYI simulations, we infer that 1/3 of the increase in the MYI+varFYI salinity is due to FYI replacing MYI, with the remaining 2/3 due to thinning snow depths on FYI.

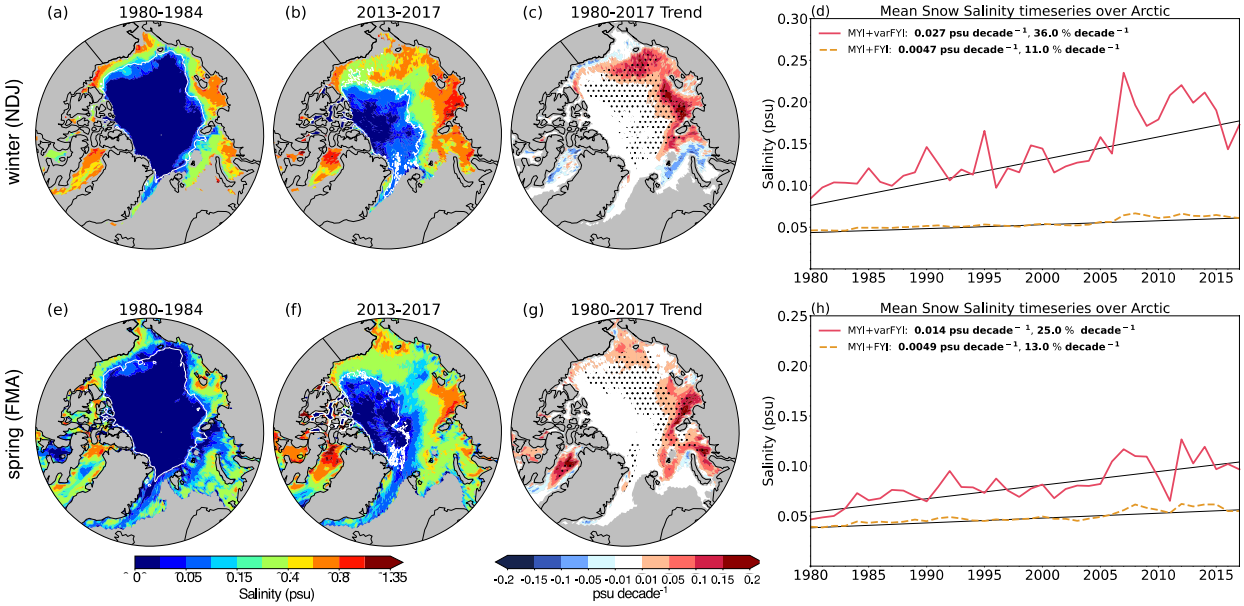

Figure 6. Seasonally averaged Arctic snow surface salinity on sea ice for winter (top row) and spring (bottom row) for the variable salinity simulation (MYI+varFYI). Average snow surface salinity for (a, e) 1980-1984 and (b, f) 2013-2017. The white contours on (a, b, e, f) show the mean extent of MYI. (c, g) Spatial distribution of trends in snow surface salinity (psu decade^{-1}) for 1980-2017. Black dots indicate statistically significant trends. (d,h) Timeseries of Arctic snow salinity for the variable salinity (MYI+varFYI, red line) and fixed salinity (MYI+FYI, orange line) simulations. The legend lists the trend in psu decade^{-1} and % decade^{-1}. Statistically significant trends are indicated in bold in the legend.

4 Changing Arctic SSA emissions and surface mass concentrations

Figure 7 (a, b and e, f) contrasts the winter and spring OO+MYI+varFYI SSA emissions for 1980-1984 and 2013-2017. Large increases in SSA emissions are predicted by the model over regions with increasing FYI. The spatial distribution of trends in SSA emissions for 1980-2017 (Figure 7c and g) show that during winter and spring, SSA trends exceed 5% decade^{-1} in regions where FYI has replaced MYI, with larger trends (>10-20% decade^{-1}) occurring over areas with the largest decreases in snow depth and increases in snow salinity.

Averaged over the Arctic region, winter and spring open ocean (OO) SSA emissions are increasing at a rate of +8.7 and +6.5% decade^{-1} (0.11 and 0.15 Tg decade^{-1}), respectively (Figure 7d, h). This is due to an increase in open water area. The OO+MYI simulation displays a weaker trend (7.5-5.1% decade^{-1}), indicating that blowing snow SSA emissions from MYI are decreasing. Adding blowing snow SSA emissions from FYI, the model predicts that total SSA emissions increase at a rate of 9.6-7.5 % decade^{-1} during winter-spring in the OO+MYI+varFYI simulation and 8.6-6.2% decade^{-1} in the OO+MYI+FYI simulation (Figure 7d, h). During winter, a large fraction of the increase in SSA emissions in the OO+MYI+varFYI (0.15 Tg decade^{-1}) is due to OO (0.11 Tg decade^{-1}), which account for 73% of SSA emissions increase. Similarly, during spring OO accounts for 62% of the increase. This is because OO emissions dominate supermicron SSA emissions (Table 1). Focusing on submicron SSA emissions, OO emissions

only account for 40% of the SSA emission increase in winter and 16% of the emission increase in spring (Figure S1). During winter and spring over the Canadian Archipelago SSA emissions are decreasing at a rate of 5-30% decade^{-1} (Figure 7c, g). In our simulation, this is driven by decreasing MERRA-2 10-meter wind speeds in that region (Figure S2). Other reanalyses also predict decreasing 10-meter wind speeds in the Canadian Archipelago (e.g., Spreen et al., 2011).

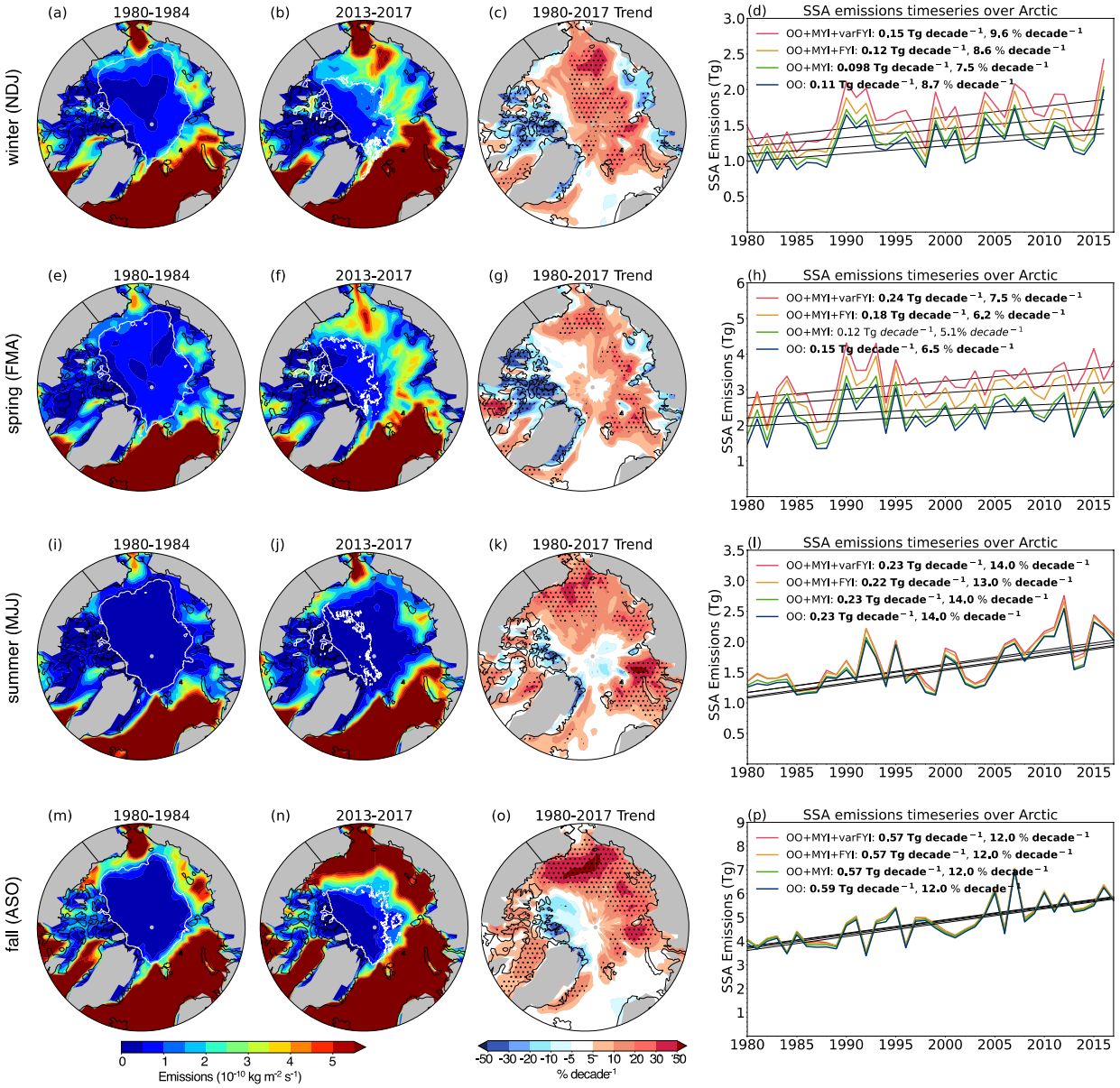

Figure 7. Seasonally averaged SSA emissions for winter (a-d), spring (e-h), summer (i-l), and fall (m-p) for the OO+MYI+varFYI simulation. The first two columns from the left indicate SSA emissions for 1980-1984 and 2013-2017. Panels c, g, k, o: Spatial distribution of 1980-2017 trends (% decade^{-1}). Black dots indicate statistically significant trends. Rightmost column (panels d, h, l, p): 1980-2017 timeseries of seasonally averaged SSA emissions over the Arctic for four simulations: OO (blue line), OO+MYI (green line), OO+MYI+FYI (orange line), OO+MYI+varFYI (red line). Note that y-axis limits differ between panels. Statistically significant trends are indicated in bold in the legend.

During the warm season, we also find that SSA emissions are increasing (Figure 7 bottom two rows), at a rate of 14% decade^{-1} in summer (MJJ) and 12% decade^{-1} in fall (ASO). In our simulations, these trends are driven by increasing open ocean emissions as MYI sea ice extent decreases.

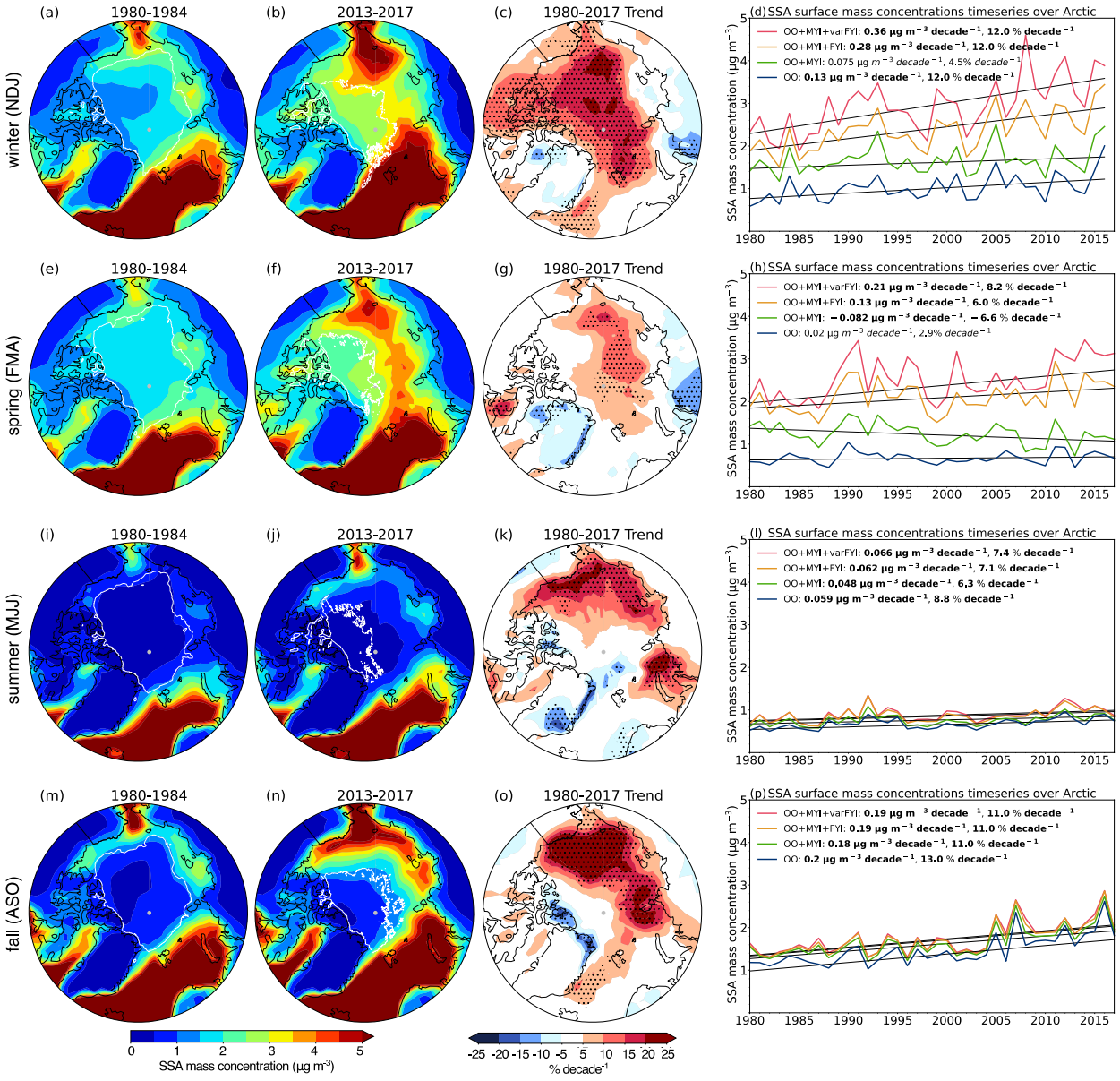

Figure 8. Same as Figure 7 but for SSA mass concentrations at the surface.

The pan-Arctic increase in SSA emissions in the OO+MYI+varFYI simulation results in statistically significant positive trends in surface SSA mass concentrations ranging from 7.4% decade^{-1} in summer to 12% decade^{-1} in winter (Figure 8 d, h, l, p). During winter, statistically significant trends exceeding 10% decade^{-1} cover most of the Arctic (Figure 8c). While the Central Arctic is dominated by MYI, trends > 5% decade^{-1} are widespread due to the transport of SSA originating from blowing snow over FYI. During spring, statistically significant trends are restricted to the central Arctic and Chukchi Sea (Figure 8g). The warm season trends are located

over regions with decreasing sea ice extent and exceed 20% decade^{-1} over many areas in fall (Figure 8o).

During winter, SSA mass concentrations due to open ocean (OO) emissions show a positive trend of 12% decade^{-1} (0.13 μg m^{-3} decade^{-1}, Figure 8d). This trend is driven by increased ocean area from decreasing MYI and delayed freeze up of FYI (Figure 4a). This positive trend counteracts the negative trend of MYI SSA surface mass concentrations in the winter, leading to nearly constant SSA from OO+MYI. During spring, when delayed freeze up of sea ice no longer impacts OO emissions, there is a much smaller trend (2.9% decade^{-1}). This results in a statistically significant negative trend in MYI+OO due to decreasing MYI emissions (Figure 8h). Thus, during both winter and spring, the positive trend in SSA mass concentrations is dominated by increasing SSA originating from blowing snow over FYI. Overall, we find that cold season (November-April) increases in blowing snow SSA account for 64-90% of the total increase in surface mass concentrations for the OO+MYI+varFYI simulation and ~54-85% in the OO+MYI+FYI simulation. During the warm season (May-October), increasing OO emissions account for more than 90% of the increase in SSA mass concentrations (Figure 8l, p).

5 Observed long-term trends in SSA mass concentrations at Alert

Alert is the only Arctic site with SSA mass concentration observations over the entire 1980-2017 period, allowing us to compare observed and simulated trends. We find that observations at Alert display positive trends of +12% decade^{-1} (+0.11 μg m^{-3} decade^{-1}) in winter and +9.6% decade^{-1} (+0.07 μg m^{-3} decade^{-1}) in spring (Figure 9a, b). These trends are significant (winter p=0.005, spring p=0.03). When sampling GEOS-Chem at Alert, both the OO+MYI+FYI and OO+MYI+varFYI simulations capture the observed interannual variability reasonably well (OO+MYI+varFYI winter r=0.7, spring r=0.59; OO+MYI+FYI winter r=0.61, spring r=0.64). These simulations predict increasing SSA mass concentrations, but the magnitude of the trends is a factor of 3-4 smaller than observed and not statistically significant. When examining the broader region surrounding Alert (Figure 8c, g), simulated trends are higher (10-15% decade^{-1}) and more consistent with observations. The weaker trends in the model at Alert relative to the modeled trends in the broader region surrounding Alert could be due to local topography effects in the model and/or the coarse horizontal resolution of the model.

During summer, observations show no trends, while the GEOS-Chem model displays weak increasing trends (<3.5%) that are not significant (Figure 9c). Fall observations display a statistically significant decreasing trend of -18% decade^{-1} (-0.036 μg m^{-3} decade^{-1}). The model simulation also predicts a decreasing trend in fall, however, it is weaker (–6% decade^{-1} to –7.5% decade^{-1}) and not significant. Figure 8o shows that in fall the model predicts that Alert is in a region of decreasing trends that extends from the Queen Elizabeth Islands to the north of Greenland, with trends ranging from -5 to -15% decade^{-1}. We find that this can be explained by statistically significant negative trends in surface winds (Figure S2) which results in decreasing SSA emissions from the open ocean (Figure 7o) in that region.

In contrast with our results, Schmale et al. (2022) analyzed observations of Na^+ from Alert but found no statistically significant trends (p>0.1) for the 1980-2017 period. While we use the same statistical method (Mann–Kendall Theil–Sen method) to calculate trends, our studies differ in the periods examined: Schmale et al. (2022) divided the year into the haze season (JFMA) and the

summer season (JJAS). The definition of these two periods follows previous studies contrasting aerosols derived from anthropogenic pollution transported to the Arctic with aerosol of a more local origin (e.g., Quinn et al., 2009). For SSA in the Arctic, our choice of four seasons aligns better with the seasonality of blowing snow and open ocean sources (Figure 3). Furthermore, Schmale et al. (2022) used seasonal median values, while we use seasonal mean values for our four seasons. We reproduce their results if we use the same seasons and medians.

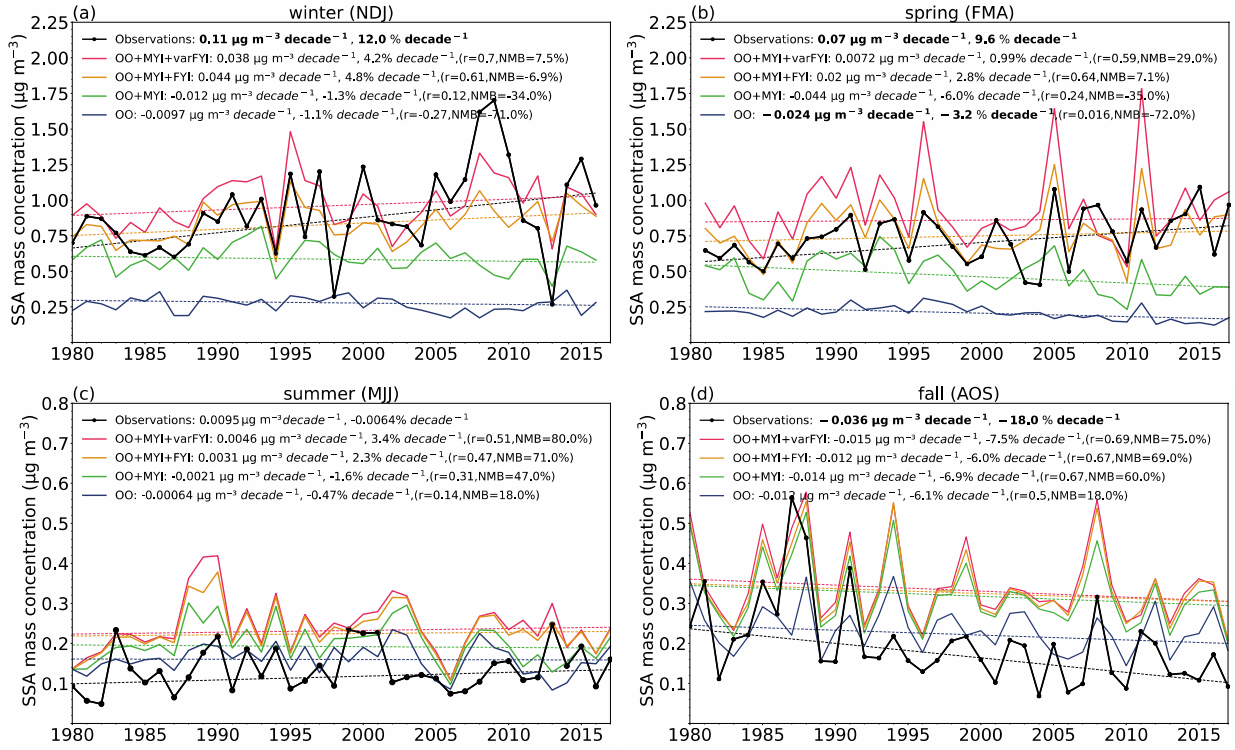

Figure 9. Seasonally averaged SSA surface mass concentrations at Alert, Canada in (a) winter (NDJ), (b) spring (FMA), (c) summer (MJJ), and (d) fall (ASO). Observations (black) and model simulations for the OO (blue line), OO+MYI (green line), OO+MYI+FYI (orange line), OO+MYI+varFYI (red line) are shown. For each panel, the legend lists the trend in μg m^{-3} (low, high) slope, and percent per decade, as well as the statistical significance (numbers in bold). For the model simulations, we include the correlation coefficient (r) and normalized mean bias (NMB) compared to observations.

6 Conclusions

We evaluated the effects of decreasing sea ice extent, age, and snow depth in the Arctic on SSA emissions and concentrations for the 1980-2017 period using the GEOS-Chem model. We conducted simulations separating the effects of SSA emissions originating from the open ocean, blowing snow on MYI, and blowing snow on FYI. For blowing snow emissions, we contrasted two simulations, one assuming fixed salinity of 0.1 psu on FYI (OO+MYI+FYI) and the other using spatially and temporally varying snow surface salinity based on an empirical salinity-snow depth relationship (OO+MYI+varFYI). Both simulations were generally successful in reproducing the observed seasonal cycle and cold season enhancement of SSA mass concentrations at four Arctic sites. However, the observations of SSA mass concentrations are

limited to areas where the OO+MYI+FYI and OO+MYI+varFYI simulations are quite similar and lack observations in areas where the simulations differ. Therefore, we cannot conclude if one simulation performs better Arctic wide. The contrast in SSA emissions between these two simulations is largest in the East Siberian, Laptev, and Kara Seas (Figure 2d, e). Thus, SSA observations in these regions would be valuable in helping to differentiate between them.

For the OO+MYI+varFYI simulation, we find that cold season pan-Arctic SSA emissions are increasing at a rate of +9.6% decade^{-1} in winter and +7.5% decade^{-1} in spring. The respective trends are +8.6% decade^{-1} and +6.2% decade^{-1} for the OO+MYI+FYI simulation. These trends in emissions are driven by a combination of decreasing sea ice extent (increasing open ocean emissions), replacement of less saline snow on MYI with more saline snow on FYI and decreasing snow depths on FYI. Our empirical snow depth-dependent salinity combined with snow depth trends from SnowModel-LG predicts a +36% decade^{-1} (0.03 psu decade^{-1}) increase in snow surface salinity during winter (+31% decade^{-1} in spring), with the largest trends in the East Siberian, Laptev, Chukchi, and Beaufort Seas. We attribute one third of this increase to the shift from MYI to FYI and the remaining two thirds to decreasing snow depths on FYI.

As a result of these increasing SSA emissions during the cold season, the OO+MYI+varFYI simulation predicts that pan-Arctic SSA surface mass concentrations have increased at a rate of +12% decade^{-1} in winter and +8.2% decade^{-1} in spring over the 1980-2017 period. The trends predicted by the OO+MYI+FYI simulation are similar (winter: +12% decade^{-1}; spring +6% decade^{-1}). These increases are driven by increasing SSA emissions from blowing snow on FYI.

We find that warm season Arctic SSA emissions are increasing at a rate of 14% decade^{-1} (summer) and 12% decade^{-1} (fall). These increases are driven by sea ice loss and the resulting increase in SSA emissions from the ice-free Arctic Ocean. Our simulations predict that SSA surface mass concentrations have increased at a rate of +7.4% decade^{-1} (summer) and 11% decade^{-1} (fall) as a result.

Observations of SSA mass concentrations at Alert for 1980-2017 display statistically significant positive trends that are of very similar magnitude to our pan-Arctic model predictions for winter (observations: +12% decade^{-1}; model: 12% decade^{-1}) and spring (observations: +9.6% decade^{-1}; model: 6-8.2% decade^{-1}). When we sample the model directly at Alert, the model underestimates the magnitude of the observed trend, potentially due to the local topography and/ or model resolution, but can reproduce the sign of the trend and the inter-annual variability. During fall, Alert observations show a negative trend of -18% decade^{-1}, which is captured by the model in the region near Alert and is driven in the model by decreasing winds speeds and thus lower SSA emissions from the open ocean.

Our finding of an increasing trend in springtime SSA concentrations over the Arctic could provide a potential explanation for the observed increase in tropospheric BrO columns over Arctic sea ice reported by Bougoudis et al. (2020). Indeed, SSA can act to release active bromine to the atmosphere, but also maintain high levels of BrO by allowing the fast recycling of sea salt bromide to reactive bromine (Abbatt et al., 2012; Fan & Jacob, 1992; Lehrer et al., 2004). Furthermore, the increasing salinity of surface snow could enhance the activation of bromine from the snowpack (Simpson et al., 2005; Pratt et al., 2013). Further studies will be needed to

642 quantitatively evaluate the impact of increasing SSA concentrations and snow surface salinity on
643 Arctic bromine activation and climate.
644

645 **Acknowledgments**

646 This work was supported under National Aeronautics and Space Administration (NASA) award
647 number 80NSSC19K1273. The authors thank Steve Warren, Becky Alexander, and Edward
648 Blanchard Wrigglesworth for helpful discussions. The authors would like to acknowledge work
649 of Dr. Len Barrie as an earlier pioneer in leading the science for the Aerosol measurements at
650 Alert, technicians/operators and Canadian Forces Alert for maintaining Alert base.

651 **Open Research**

652 The EASE-Grid Sea Ice Age data is available online (https://nsidc.org/data/nsidc-
653 0611/versions/4). Daily, 1 September 1980 through 31 July 2018, snow depths used in this paper
654 are available at the National Snow and Ice Data Center (NSIDC), Boulder, Colorado USA:
655 Liston, G. E., J. Stroeve, and P. Itkin; Lagrangian Snow Distributions for Sea-Ice Applications;
656 http://dx.doi.org/10.5067/27A0P5M6LZBI.

657 **References**

658 Abbatt, J. P. D., R. Leaitch, W., Aliabadi, A. A., Bertram, A. K., Blanchet, J. P., Boivin-Rioux,
659 A., Bozem, H., Burkart, J., Chang, R. Y. W., Charette, J., Chaubey, J. P., Christensen, R. J.,
660 Cirisan, A., Collins, D. B., Croft, B., Dionne, J., Evans, G. J., Fletcher, C. G., Gali, M., …
661 Yakobi-Hancock, J. D. (2019). Overview paper: New insights into aerosol and climate in
662 the Arctic. *Atmospheric Chemistry and Physics*, *19*(4). https://doi.org/10.5194/acp-19-2527-
663 2019
664 Abbatt, J. P. D., Thomas, J. L., Abrahamsson, K., Boxe, C., Granfors, A., Jones, A. E., King, M.
665 D., Saiz-Lopez, A., Shepson, P. B., Sodeau, J., Toohey, D. W., Toubin, C., von Glasow, R.,
666 Wren, S. N., & Yang, X. (2012). Halogen activation via interactions with environmental ice
667 and snow in the polar lower troposphere and other regions. *Atmospheric Chemistry and*
668 *Physics*, *12*(14), 6237–6271. https://doi.org/10.5194/acp-12-6237-2012

669 Alvarez-Aviles, L., Simpson, W. R., Douglas, T. A., Sturm, M., Perovich, D., & Domine, F.
670 (2008). Frost flower chemical composition during growth and its implications for aerosol
671 production and bromine activation. *Journal of Geophysical Research Atmospheres*, *113*(21).
672 https://doi.org/10.1029/2008JD010277
673 Bey, I., Jacob, D. J., Yantosca, R. M., Logan, J. A., Field, B. D., Fiore, A. M., Li, Q., Liu, H. Y.,
674 Mickley, L. J., & Schultz, M. G. (2001). Global modeling of tropospheric chemistry with
675 assimilated meteorology: Model description and evaluation. *Journal of Geophysical*
676 *Research Atmospheres*, *106*(D19). https://doi.org/10.1029/2001JD000807
677 Bougoudis, I., Blechschmidt, A. M., Richter, A., Seo, S., Burrows, J. P., Theys, N., & Rinke, A.
678 (2020). Long-term time series of Arctic tropospheric BrO derived from UV-VIS satellite
679 remote sensing and its relation to first-year sea ice. *Atmospheric Chemistry and Physics*.
680 https://doi.org/10.5194/acp-20-11869-2020
681 Browse, J., Carslaw, K. S., Mann, G. W., Birch, C. E., Arnold, S. R., & Leck, C. (2014). The
682 complex response of Arctic aerosol to sea-ice retreat. *Atmospheric Chemistry and Physics*,
683 *14*(14). https://doi.org/10.5194/acp-14-7543-2014
684 Budd, W. F. (2013). *The Drifting of Nonuniform Snow Particles 1* .
685 https://doi.org/10.1029/ar009p0059
686 Choi, S., Theys, N., Salawitch, R. J., Wales, P. A., Joiner, J., Canty, T. P., Chance, K., Suleiman,
687 R. M., Palm, S. P., Cullather, R. I., Darmenov, A. S., da Silva, A., Kurosu, T. P., Hendrick,
688 F., & van Roozendael, M. (2018). Link Between Arctic Tropospheric BrO Explosion
689 Observed From Space and Sea-Salt Aerosols From Blowing Snow Investigated Using
690 Ozone Monitoring Instrument BrO Data and GEOS-5 Data Assimilation System. *Journal of*
691 *Geophysical Research: Atmospheres*. https://doi.org/10.1029/2017JD026889

692 Collaud Coen, M., Andrews, E., Bigi, A., Martucci, G., Romanens, G., Vogt, F. P. A., &
693 Vuilleumier, L. (2020a). Effects of the prewhitening method, the time granularity, and the
694 time segmentation on the Mann-Kendall trend detection and the associated Sen's slope.
695 *Atmospheric Measurement Techniques*, *13*(12). https://doi.org/10.5194/amt-13-6945-2020
696 Collaud Coen, M., Andrews, E., Lastuey, A., Petkov Arsov, T., Backman, J., Brem, B. T.,
697 Bukowiecki, N., Couret, C., Eleftheriadis, K., Flentje, H., Fiebig, M., Gysel-Beer, M.,
698 Hand, J. L., Hoffer, A., Hooda, R., Hueglin, C., Joubert, W., Keywood, M., Eun Kim, J., …
699 Laj, P. (2020b). Multidecadal trend analysis of in situ aerosol radiative properties around
700 the world. *Atmospheric Chemistry and Physics*, *20*(14). https://doi.org/10.5194/acp-20-
701 8867-2020
702 Cox, G. F. N., & Weeks, W. F. (1974). Salinity Variations in Sea Ice. *Journal of Glaciology*,
703 *13*(67), 109–120. https://doi.org/10.3189/S0022143000023418
704 de Leeuw, G., Andreas, E. L., Anguelova, M. D., Fairall, C. W., Lewis, E. R., O'Dowd, C.,
705 Schulz, M., & Schwartz, S. E. (2011). Production flux of sea spray aerosol. *Reviews of*
706 *Geophysics*, *49*(2). https://doi.org/10.1029/2010RG000349
707 DeMott, P. J., Hill, T. C. J., McCluskey, C. S., Prather, K. A., Collins, D. B., Sullivan, R. C.,
708 Ruppel, M. J., Mason, R. H., Irish, V. E., Lee, T., Hwang, C. Y., Rhee, T. S., Snider, J. R.,
709 McMeeking, G. R., Dhaniyala, S., Lewis, E. R., Wentzell, J. J. B., Abbatt, J., Lee, C., …
710 Franc, G. D. (2016). Sea spray aerosol as a unique source of ice nucleating particles.
711 *Proceedings of the National Academy of Sciences of the United States of America*, *113*(21).
712 https://doi.org/10.1073/pnas.1514034112
713 Déry, S. J., & Yau, M. K. (1999). A bulk blowing snow model. *Boundary-Layer Meteorology*,
714 *93*(2). https://doi.org/10.1023/A:1002065615856

Domine, F., Sparapani, R., Ianniello, A., & Beine, H. J. (2004). The origin of sea salt in snow on Arctic sea ice and in coastal regions. *Atmospheric Chemistry and Physics*, *4*(9–10). https://doi.org/10.5194/acp-4-2259-2004

Donlon, C. J., Martin, M., Stark, J., Roberts-Jones, J., Fiedler, E., & Wimmer, W. (2012). The Operational Sea Surface Temperature and Sea Ice Analysis (OSTIA) system. *Remote Sensing of Environment*, *116*. https://doi.org/10.1016/j.rse.2010.10.017

Drinkwater, M. R., & Crocker, G. B. (1988). Modelling changes in the dielectric and scattering properties of young snow-covered sea ice at GHz frequencies. *Journal of Glaciology*, *34*(118). https://doi.org/10.3189/s0022143000007012

Ewert, M., Carpenter, S. D., Colangelo-Lillis, J., & Deming, J. W. (2013). Bacterial and extracellular polysaccharide content of brine-wetted snow over Arctic winter first-year sea ice. *Journal of Geophysical Research: Oceans*. https://doi.org/10.1002/jgrc.20055

Fan, S. M., & Jacob, D. J. (1992). Surface ozone depletion in Arctic spring sustained by bromine reactions on aerosols. *Nature*, *359*(6395). https://doi.org/10.1038/359522a0

Fisher, J. A., Jacob, D. J., Wang, Q., Bahreini, R., Carouge, C. C., Cubison, M. J., Dibb, J. E., Diehl, T., Jimenez, J. L., Leibensperger, E. M., Lu, Z., Meinders, M. B. J., Pye, H. O. T., Quinn, P. K., Sharma, S., Streets, D. G., van Donkelaar, A., & Yantosca, R. M. (2011). Sources, distribution, and acidity of sulfate-ammonium aerosol in the Arctic in winter-spring. *Atmospheric Environment*, *45*(39). https://doi.org/10.1016/j.atmosenv.2011.08.030

Fox-Kemper, B., Hewitt, H., Xiao, C., Aðalgeirsdóttir, G., Drijfhout, S., Edwards, T., Golledge, N., Hemer, M., Kopp, R., Krinner, G., Mix, A., Notz, D., Nowiciki, S., Nurhati, I., Ruiz, J., Sallée, J., Slangen, A., & Yu, Y. (2021). Ocean, Cryosphere and Sea Level Change. Climate Change 2021: The Physical Science Basis. Contribution of Working Group I to the Sixth

738 Assessment Report of the Intergovernmental Panel on Climate Change. Cambridge Univ.
739 Press, Cambridge, United Kingdom and New York, NY, USA, pp. 1211-1362.
740 doi:10.1017/9781009157896.011
741 Freud, E., Krejci, R., Tunved, P., Leaitch, R., Nguyen, Q. T., Massling, A., Skov, H., & Barrie,
742 L. (2017). Pan-Arctic aerosol number size distributions: Seasonality and transport patterns.
743 *Atmospheric Chemistry and Physics*, *17*(13). https://doi.org/10.5194/acp-17-8101-2017
744 Frey, M., Norris, S., Brooks, I., Anderson, P., Nishimura, K., Yang, X., Jones, A., Nerentorp
745 Mastromonaco, M., Jones, D., & Wolff, E. (2019). First direct observation of sea salt
746 aerosol production from blowing snow above sea ice. *Atmospheric Chemistry and Physics*.
747 https://doi.org/10.5194/acp-2019-259
748 Gelaro, R., McCarty, W., Suárez, M. J., Todling, R., Molod, A., Takacs, L., Randles, C. A.,
749 Darmenov, A., Bosilovich, M. G., Reichle, R., Wargan, K., Coy, L., Cullather, R., Draper,
750 C., Akella, S., Buchard, V., Conaty, A., da Silva, A. M., Gu, W., … Zhao, B. (2017). The
751 modern-era retrospective analysis for research and applications, version 2 (MERRA-2).
752 *Journal of Climate*. https://doi.org/10.1175/JCLI-D-16-0758.1
753 Geldsetzer, T., Langlois, A., & Yackel, J. (2009). Dielectric properties of brine-wetted snow on
754 first-year sea ice. *Cold Regions Science and Technology*, 58(1-2), 47-56.
755 doi:10.1016/j.coldregions.2009.03.009
756 Gilgen, A., Ting Katty Huang, W., Ickes, L., Neubauer, D., & Lohmann, U. (2018). How
757 important are future marine and shipping aerosol emissions in a warming Arctic summer
758 and autumn? *Atmospheric Chemistry and Physics*, *18*(14). https://doi.org/10.5194/acp-18-
759 10521-2018

760 Giordano, M. R., Kalnajs, L. E., Goetz, J. D., Avery, A. M., Katz, E., May, N. W., Leemon, A.,
761 Mattson, C., Pratt, K. A., & DeCarlo, P. F. (2018). The importance of blowing snow to
762 halogen-containing aerosol in coastal Antarctica: Influence of source region versus wind
763 speed. Atmospheric Chemistry and Physics, 18(22), 16,689–16,711. https://doi-org
764 /10.5194/acp-18-16689-2018
765 Heslin-Rees, D., Burgos, M., Hansson, H. C., Krejci, R., Ström, J., Tunved, P., & Zieger, P.
766 (2020). From a polar to a marine environment: Has the changing Arctic led to a shift in
767 aerosol light scattering properties? *Atmospheric Chemistry and Physics*, *20*(21).
768 https://doi.org/10.5194/acp-20-13671-2020
769 Huang, J., & Jaeglé, L. (2017). Wintertime enhancements of sea salt aerosol in polar regions
770 consistent with a sea ice source from blowing snow. *Atmospheric Chemistry and Physics*,
771 *17*(5). https://doi.org/10.5194/acp-17-3699-2017
772 Huang, J., Jaeglé, L., & Shah, V. (2018). Using CALIOP to constrain blowing snow emissions of
773 sea salt aerosols over Arctic and Antarctic sea ice. *Atmospheric Chemistry and Physics*,
774 *18*(22), 16253–16269. https://doi.org/10.5194/acp-18-16253-2018
775 Huang, J., Jaeglé, L., Chen, Q., Alexander, B., Sherwen, T., Evans, M. J., Theys, N., & Choi, S.
776 (2020). Evaluating the impact of blowing-snow sea salt aerosol on springtime BrO and O3
777 in the Arctic. *Atmospheric Chemistry and Physics*, *20*(12), 7335–7358.
778 https://doi.org/10.5194/acp-20-7335-2020
779 Jaeglé, L., Quinn, P. K., Bates, T. S., Alexander, B., & Lin, J. T. (2011). Global distribution of
780 sea salt aerosols: New constraints from in situ and remote sensing observations.
781 *Atmospheric Chemistry and Physics*, *11*(7). https://doi.org/10.5194/acp-11-3137-2011

Kaleschke, L., Richter, A., Burrows, J., Afe, O., Heygster, G., Notholt, J., Rankin, A. M., Roscoe, H. K., Hollwedel, J., Wagner, T., & Jacobi, H. W. (2004). Frost flowers on sea ice as a source of sea salt and their influence on tropospheric halogen chemistry. *Geophysical Research Letters*. https://doi.org/10.1029/2004GL020655

Kalnajs, L. E., Avallone, L. M., & Toohey, D. W. (2013). Correlated measurements of ozone and particulates in the Ross Island region, Antarctica. *Geophysical Research Letters*, *40*(23). https://doi.org/10.1002/2013GL058422

Keller, C. A., Long, M. S., Yantosca, R. M., da Silva, A. M., Pawson, S., & Jacob, D. J. (2014). HEMCO v1.0: A versatile, ESMF-compliant component for calculating emissions in atmospheric models. *Geoscientific Model Development*. https://doi.org/10.5194/gmd-7-1409-2014

Krnavek, L., Simpson, W. R., Carlson, D., Domine, F., Douglas, T. A., & Sturm, M. (2012). The chemical composition of surface snow in the Arctic: Examining marine, terrestrial, and atmospheric influences. *Atmospheric Environment*. https://doi.org/10.1016/j.atmosenv.2011.11.033

Kwok, R. (2018). Arctic sea ice thickness, volume, and multiyear ice coverage: Losses and coupled variability (1958-2018). In *Environmental Research Letters* (Vol. 13, Issue 10). https://doi.org/10.1088/1748-9326/aae3ec

Lam, H. M., Geldsetzer, T., Howell, S. E. L, and Yackel, J. (2022). Snow Depth on Sea Ice and on Land in the Canadian Arctic from Long-Term Observations, Atmosphere-Ocean, doi: 10.1080/07055900.2022.2060178

Lehrer, E., Hönninger, G., & Platt, U. (2004). A one dimensional model study of the mechanism of halogen liberation and vertical transport in the polar troposphere. *Atmospheric Chemistry and Physics*, *4*(11–12). https://doi.org/10.5194/acp-4-2427-2004

Lewis, E. R., & Schwartz, S. E. (2004). Sea salt aerosol production: Mechanisms, methods, measurements and models—A critical review. In *Geophysical Monograph Series* (Vol. 152). https://doi.org/10.1029/152GM01

Liston, G. E., Itkin, P., Stroeve, J., Tschudi, M., Stewart, J. S., Pedersen, S. H., Reinking, A. K., & Elder, K. (2020). A Lagrangian Snow-Evolution System for Sea-Ice Applications (SnowModel-LG): Part I—Model Description. *Journal of Geophysical Research: Oceans*, *125*(10). https://doi.org/10.1029/2019JC015913

Liston, G. E., & Sturm, M. (2002). Winter precipitation patterns in arctic Alaska determined from a blowing-snow model and snow-depth observations. *Journal of Hydrometeorology*, *3*(6). https://doi.org/10.1175/1525-7541(2002)003<0646:WPPIAA>2.0.CO;2

Liu, H., Jacob, D. J., Bey, I., & Yantosca, R. M. (2001). Constraints from 210Pb and 7Be on wet deposition and transport in a global three-dimensional chemical tracer model driven by assimilated meteorological fields. *Journal of Geophysical Research Atmospheres*, *106*(D11). https://doi.org/10.1029/2000JD900839

Mallett, R. D. C., Stroeve, J. C., Tsamados, M., Landy, J. C., Willatt, R., Nandan, V., & Liston, G. E. (2021). Faster decline and higher variability in the sea ice thickness of the marginal Arctic seas when accounting for dynamic snow cover. *Cryosphere*, *15*(5). https://doi.org/10.5194/tc-15-2429-2021

824 Mann, G. W., Anderson, P. S., & Mobbs, S. D. (2000). Profile measurements of blowing snow at
825 Halley, Antarctica. *Journal of Geophysical Research Atmospheres*, *105*(D19).
826 https://doi.org/10.1029/2000JD900247
827 Marelle, L., Thomas, J. L., Ahmed, S., Tuite, K., Stutz, J., Dommergue, A., Simpson, W. R.,
828 Frey, M. M., & Baladima, F. (2021). Implementation and Impacts of Surface and Blowing
829 Snow Sources of Arctic Bromine Activation Within WRF-Chem 4.1.1. *Journal of Advances*
830 *in Modeling Earth Systems*, *13*(8). https://doi.org/10.1029/2020MS002391
831 Markus, T., Stroeve, J. C., & Miller, J. (2009). Recent changes in Arctic sea ice melt onset,
832 freezeup, and melt season length. *Journal of Geophysical Research: Oceans*, *114*(12).
833 https://doi.org/10.1029/2009JC005436
834 Massom, R. A., Eicken, H., Haas, C., Jeffries, M. O., Drinkwater, M. R., Sturm, M., Worby, A.
835 P., Wu, X., Lytle, V. I., Ushio, S., Morris, K., Reid, P. A., Warren, S. G., & Allison, I.
836 (2001). Snow on Antarctic sea ice. *Reviews of Geophysics*, *39*(3).
837 https://doi.org/10.1029/2000RG000085
838 May, N. W., Quinn, P. K., McNamara, S. M., & Pratt, K. A. (2016). Multiyear study of the
839 dependence of sea salt aerosol on wind speed and sea ice conditions in the coastal Arctic.
840 *Journal of Geophysical Research: Atmospheres*, *121(15)*, 9208–9219.
841 https://doi.org/10.1002/2016JD025273
842 Meredith, M., Sommerkorn, M., Cassotta, S., Derksen, C., Ekaykin, A., Hollowed, A., Kofinas,
843 G., Mackintosh, A., Melbourne-Thomas, J., Muelbert, M.M.C., Ottersen, G., Pritchard, H.,
844 and Schuur, E.A.G. (2019). Polar Regions. In: IPCC Special Report on the Ocean and
845 Cryosphere in a Changing Climate [H.-O. Pörtner, D.C. Roberts, V. MassonDelmotte, P.
846 Zhai, M. Tignor, E. Poloczanska, K. Mintenbeck, A. Alegría, M. Nicolai, A. Okem, J.

Petzold, B. Rama, N.M. Weyer (eds.)]. Cambridge University Press, Cambridge, UK and New York, NY, USA, pp. 203-320. https://doi.org/10.1017/9781009157964.005.

Moschos, V., Schmale, J., Aas, W., Becagli, S., Calzolai, G., Eleftheriadis, K., Moffett, C. E., Schnelle-Kreis, J., Severi, M., Sharma, S., Skov, H., Vestenius, M., Zhang, W., Hakola, H., Hellén, H., Huang, L., Jaffrezo, J.-L., Massling, A., Nøjgaard, J. K., Petäjä, T., Popovicheva, O., Sheesley, R. J., Traversi, R., Yttri, K. E., Prévôt, A. S. H., Baltensperger, U., and Haddad, I. E. (2022). Elucidating the present-day chemical composition, seasonality and source regions of climate-relevant aerosols across the Arctic land surface. *Environmental Research Letters*, *17*, 034032. https://doi.org/10.1088/1748-9326/ac444b

Nandan, V., Scharien, R., Geldsetzer, T., Mahmud, M., Yackel, J. J., Islam, T., ... & Duguay, C. (2017a). Geophysical and atmospheric controls on Ku-, X-and C-band backscatter evolution from a saline snow cover on first-year sea ice from late-winter to pre-early melt. *Remote Sensing of Environment*, *198*, 425-441. https://doi.org/10.1016/j.rse.2017.06.029

Nandan, V., Geldsetzer, T., Yackel, J., Mahmud, M., Scharien, R., Howell, S., King, J., Ricker, R., & Else, B. (2017b). Effect of Snow Salinity on CryoSat-2 Arctic First-Year Sea Ice Freeboard Measurements. *Geophysical Research Letters*. https://doi.org/10.1002/2017GL074506

Nilsson, E. D., Rannik, Ü., Swietlicki, E., Leck, C., Aalto, P. P., Zhou, J., & Norman, M. (2001). Turbulent aerosol fluxes over the Arctic Ocean 2. Wind-driven sources from the sea. *Journal of Geophysical Research Atmospheres*, *106*(D23). https://doi.org/10.1029/2000JD900747

868 Nishimura, K., & Nemoto, M. (2005). Blowing snow at Mizuho station, Antarctica.
869 *Philosophical Transactions of the Royal Society A: Mathematical, Physical and*
870 *Engineering Sciences*, *363*(1832). https://doi.org/10.1098/rsta.2005.1599
871 O'Dowd, C. D., Smith, M. H., Consterdine, I. E., & Lowe, J. A. (1997). Marine aerosol, sea-salt,
872 and the marine sulphur cycle: A short review. *Atmospheric Environment*, *31*(1).
873 https://doi.org/10.1016/S1352-2310(96)00106-9
874 Parkinson, C. L., & Comiso, J. C. (2013). On the 2012 record low Arctic sea ice cover:
875 Combined impact of preconditioning and an August storm. *Geophysical Research Letters*,
876 *40*(7). https://doi.org/10.1002/grl.50349
877 Perovich, D. K., & Richter-Menge, J. A. (1994). Surface characteristics of lead ice. *Journal of*
878 *Geophysical Research*, *99*(C8). https://doi.org/10.1029/94jc01194
879 Peterson, P. K., Hartwig, M., May, N. W., Schwartz, E., Rigor, I., Ermold, W., Steele, M.,
880 Morison, J. H., Nghiem, S. v., & Pratt, K. A. (2019). Snowpack measurements suggest role
881 for multi-year sea ice regions in Arctic atmospheric bromine and chlorine chemistry.
882 *Elementa*, *7*(1). https://doi.org/10.1525/elementa.352
883 Pratt, K. A., Custard, K. D., Shepson, P. B., Douglas, T. A., Poehler, D., General, S., Zielcke, J.,
884 Simpson, W. R., Platt, U., Tanner, D. J., Huey, L. G., Carlsen, M., & Stirm, B. H. (2013).
885 Photochemical production of molecular bromine in Arctic surface snowpacks. *Nature*
886 *Geoscience*, *6(5)*, 351–356. https://doi.org/10.1038/NGEO1779
887 Quinn, P. K., Bates, T. S., Schulz, K., & Shaw, G. E. (2009). Decadal trends in aerosol chemical
888 composition at Barrow, Alaska: 1976–2008. *Atmospheric Chemistry and Physics*, *9(22)*,
889 8883–8888. https://doi.org/10.5194/acp-9-8883-2009

Quinn, P. K., Miller, T. L., Bates, T. S., Ogren, J. A., Andrews, E., & Shaw, G. E. (2002). A 3-year record of simultaneously measured aerosol chemical and optical properties at Barrow, Alaska. *Journal of Geophysical Research: Atmospheres*, *107(D11)*, AAC 8-1-AAC 8-15. https://doi.org/10.1029/2001JD001248

Rankin, A. M., Wolff, E. W., & Martin, S. (2002). Frost flowers: Implications for tropospheric chemistry and ice core interpretation. *Journal of Geophysical Research Atmospheres*. https://doi.org/10.1029/2002JD002492

Reynolds, R. W., Smith, T. M., Liu, C., Chelton, D. B., Casey, K. S., & Schlax, M. G. (2007). Daily high-resolution-blended analyses for sea surface temperature. *Journal of Climate*, *20*(22). https://doi.org/10.1175/2007JCLI1824.1

Rhodes, R. H., Yang, X., Wolff, E. W., McConnell, J. R., & Frey, M. M. (2017). Sea ice as a source of sea salt aerosol to Greenland ice cores: A model-based study. *Atmospheric Chemistry and Physics*, *17*(15). https://doi.org/10.5194/acp-17-9417-2017

Riley, J. P. and Chester, R. (1971). Introduction to Marine Chemistry, Academic, New York.

Roscoe, H. K., Brooks, B., Jackson, A. v., Smith, M. H., Walker, S. J., Obbard, R. W., & Wolff, E. W. (2011). Frost flowers in the laboratory: Growth, characteristics, aerosol, and the underlying sea ice. *Journal of Geophysical Research Atmospheres*, *116*(12). https://doi.org/10.1029/2010JD015144

Schmale, J., Zieger, P., & Ekman, A. M. L. (2021). Aerosols in current and future Arctic climate. *Nature Climate Change*, *11*(2). https://doi.org/10.1038/s41558-020-00969-5

Schmale, J., Sharma, S., Decesari, S., Pernov, J., Massling, A., Hansson, H.-C., von Salzen, K., Skov, H., Andrews, E., Quinn, P. K., Upchurch, L. M., Eleftheriadis, K., Traversi, R., Gilardoni, S., Mazzola, M., Laing, J., & Hopke, P. (2022). Pan-Arctic seasonal cycles and

913 long-term trends of aerosol properties from 10 observatories. *Atmospheric Chemistry and*
914 *Physics, 22(5),* 3067–3096. https://doi.org/10.5194/acp-22-3067-2022
915 Sharma, S., Barrie, L. A., Magnusson, E., Brattström, G., Leaitch, W. R., Steffen, A., &
916 Landsberger, S. (2019). A Factor and Trends Analysis of Multidecadal Lower Tropospheric
917 Observations of Arctic Aerosol Composition, Black Carbon, Ozone, and Mercury at Alert,
918 Canada. *Journal of Geophysical Research: Atmospheres*, *124*(24).
919 https://doi.org/10.1029/2019JD030844
920 Simpson, W. R., Alvarez-Aviles, L., Douglas, T. A., Sturm, M., & Domine, F. (2005). Halogens
921 in the coastal snow pack near Barrow, Alaska: Evidence for active bromine air-snow
922 chemistry during springtime. *Geophysical Research Letters*, *32(4)*.
923 https://doi.org/10.1029/2004GL021748
924 Simpson, W. R., von Glasow, R., Riedel, K., Anderson, P., Ariya, P., Bottenheim, J., Burrows,
925 J., Carpenter, L. J., Frieß, U., Goodsite, M. E., Heard, D., Hutterli, M., Jacobi, H. W.,
926 Kaleschke, L., Neff, B., Plane, J., Platt, U., Richter, A., Roscoe, H., … Wolff, E. (2007).
927 Halogens and their role in polar boundary-layer ozone depletion. *Atmospheric Chemistry*
928 *and Physics*, *7*(16), 4375–4418. https://doi.org/10.5194/acp-7-4375-2007
929 Skov, H., Hjorth, J., Nordstrøm, C., Jensen, B., Christoffersen, C., Poulsen, M. B., Liisberg, J.
930 B., Beddows, D., Dall'Osto, M., & Christensen, J. H. (2020). Variability in gaseous
931 elemental mercury at villum research station, Station Nord, in North Greenland from 1999
932 to 2017. *Atmospheric Chemistry and Physics*, *20*(21). https://doi.org/10.5194/acp-20-13253-
933 2020
934 Slinn, S. A., & Slinn, W. G. N. (1980). Predictions for particle deposition on natural waters.
935 *Atmospheric Environment (1967)*, *14*(9). https://doi.org/10.1016/0004-6981(80)90032-3

936 Spreen, G., Kwok, R., and Menemenlis, D. (2011). Trends in Arctic sea ice drift and role of wind
937 forcing: 1992–2009. *Geophysical Research Letters, 38*.
938 https://doi.org/10.1029/2011GL048970
939 Stroeve, J., Liston, G. E., Buzzard, S., Zhou, L., Mallett, R., Barrett, A., Tschudi, M., Tsamados,
940 M., Itkin, P., & Stewart, J. S. (2020). A Lagrangian Snow Evolution System for Sea Ice
941 Applications (SnowModel-LG): Part II—Analyses. *Journal of Geophysical Research:*
942 *Oceans*, *125*(10). https://doi.org/10.1029/2019JC015900
943 Stroeve, J., & Notz, D. (2018). Changing state of Arctic sea ice across all seasons. In
944 *Environmental Research Letters* (Vol. 13, Issue 10). https://doi.org/10.1088/1748-
945 9326/aade56
946 Struthers, H., Ekman, A. M. L., Glantz, P., Iversen, T., Kirkevåg, A., Mårtensson, E. M., Seland,
947 & Nilsson, E. D. (2011). The effect of sea ice loss on sea salt aerosol concentrations and the
948 radiative balance in the Arctic. *Atmospheric Chemistry and Physics*, *11*(7).
949 https://doi.org/10.5194/acp-11-3459-2011
950 Swanson, W. F., Holmes, C. D., Simpson, W. R., Confer, K., Marelle, L., Thomas, J. L., Jaeglé,
951 L., Alexander, B., Zhai, S., Chen, Q., Wang, X., & Sherwen, T. (2022). Comparison of
952 model and ground observations finds snowpack and blowing snow both contribute to Arctic
953 tropospheric reactive bromine. *Atmospheric Chemistry and Physics Discussions*, 1–38.
954 https://doi.org/10.5194/acp-2022-44
955 Taylor, K. E., Williamson, D. L., & Zwiers, F. W. (2000). The Sea Surface Temperature and
956 Sea-Ice Concentration Boundary Conditions for AMIP II Simulations. *PCMDI Report*
957 *Series*, *60*.

Tørseth, K., Aas, W., Breivik, K., Fjeraa, A. M., Fiebig, M., Hjellbrekke, A. G., Lund Myhre, C., Solberg, S., & Yttri, K. E. (2012). Introduction to the European Monitoring and Evaluation Programme (EMEP) and observed atmospheric composition change during 1972-2009. In *Atmospheric Chemistry and Physics* (Vol. 12, Issue 12). https://doi.org/10.5194/acp-12-5447-2012

Tschudi, M. A., Meier, W. N., & Scott Stewart, J. (2020). An enhancement to sea ice motion and age products at the National Snow and Ice Data Center (NSIDC). *Cryosphere*, *14*(5). https://doi.org/10.5194/tc-14-1519-2020

Tschudi, M., Meier, W. N., Stewart, J. S., Fowler, C., & Maslanik, J. (2019). EASE-Grid Sea Ice Age, Version 4. In *NASA National Snow and Ice Data Center Distributed Active Archive Center*. https://doi.org/10.5067/UTAV7490FEPB

Tunved, P., & Ström, J. (2019). On the seasonal variation in observed size distributions in northern Europe and their changes with decreasing anthropogenic emissions in Europe: Climatology and trend analysis based on 17 years of data from Aspvreten, Sweden. *Atmospheric Chemistry and Physics*, *19*(23). https://doi.org/10.5194/acp-19-14849-2019

Wang, Q., Jacob, D. J., Fisher, J. A., Mao, J., Leibensperger, E. M., Carouge, C. C., le Sager, P., Kondo, Y., Jimenez, J. L., Cubison, M. J., & Doherty, S. J. (2011). Sources of carbonaceous aerosols and deposited black carbon in the Arctic in winter-spring: Implications for radiative forcing. *Atmospheric Chemistry and Physics*, *11*(23). https://doi.org/10.5194/acp-11-12453-2011

Webster, M. A., Rigor, I. G., Nghiem, S. v., Kurtz, N. T., Farrell, S. L., Perovich, D. K., & Sturm, M. (2014). Interdecadal changes in snow depth on Arctic sea ice. *Journal of Geophysical Research: Oceans*, *119*(8). https://doi.org/10.1002/2014jc009985

Wise, M. E., Baustian, K. J., Koop, T., Freedman, M. A., Jensen, E. J., & Tolbert, M. A. (2012). Depositional ice nucleation onto crystalline hydrated NaCl particles: A new mechanism for ice formation in the troposphere. *Atmospheric Chemistry and Physics*, *12*(2), 1121–1134. https://doi.org/10.5194/acp-12-1121-2012

Yang, X., Frey, M. M., Rhodes, R. H., Norris, S. J., Brooks, I. M., Anderson, P. S., Nishimura, K., Jones, A. E., & Wolff, E. W. (2019). Sea salt aerosol production via sublimating wind-blown saline snow particles over sea ice: Parameterizations and relevant microphysical mechanisms. *Atmospheric Chemistry and Physics*, *19*(13), 8407–8424. https://doi.org/10.5194/acp-19-8407-2019

Yang, X., Neděla, V., Runštuk, J., Ondrušková, G., Krausko, J., Vetráková, L., & Heger, D. (2017). Evaporating brine from frost flowers with electron microscopy and implications for atmospheric chemistry and sea-salt aerosol formation. *Atmospheric Chemistry and Physics*, *17*(10). https://doi.org/10.5194/acp-17-6291-2017

Yang, X., Pyle, J. A., & Cox, R. A. (2008). Sea salt aerosol production and bromine release: Role of snow on sea ice. *Geophysical Research Letters*. https://doi.org/10.1029/2008GL034536

Yang, X., Pyle, J. A., Cox, R. A., Theys, N., & van Roozendael, M. (2010). Snow-sourced bromine and its implications for polar tropospheric ozone. *Atmospheric Chemistry and Physics*, *10*(16), 7763–7773. https://doi.org/10.5194/acp-10-7763-2010

Zhang, L., Gong, S., Padro, J., & Barrie, L. (2001). A size-segregated particle dry deposition scheme for an atmospheric aerosol module. *Atmospheric Environment*, *35*(3). https://doi.org/10.1016/S1352-2310(00)00326-5